

Supporting Information

Self-Templated Generation of Triggerable and Restorable Nonequilibrium Micelles

Claudia Dähling, Judith E. Houston, Aurel Radulescu, Markus Drechsler, Monia Brugnoli, Hideharu Mori, Dmitry V. Pergushov, and Felix A. Plamper*

Abstract: Conditional variations can lead to micellar transformations resulting in various (equilibrium) morphologies. However, creating differently shaped assemblies under the same final conditions (same ingredients, composition, temperature, etc.) is challenging. We present a thermoresponsive polyelectrolyte system allowing a pathway-dependent preparation of kinetically stable spherical star-like or cylindrical micelles. In more detail, a temperature-induced structure switch is used to generate equilibrated interpolyelectrolyte complex (IPEC) micelles of different morphologies (templates) below and above the lower critical solution temperature in presence of plasticizer (salt). Then, lowering the salt concentration at a specific temperature kinetically freezes the formed IPECs, keeping the respective microstructural information encoded in the frozen IPEC also at other temperatures. Hence, different nonequilibrium morphologies at the same final conditions are provided. The salt-triggered transition from nonequilibrium to equilibrium micelles can be repeated for the same sample, highlighting a system with an on-demand changeable and restorable structure.

Table of Contents

Table of Contents	2
1. Experimental Procedures.....	3
1.1. Sample Preparation.....	3
1.2. Dynamic Light Scattering.....	4
1.3. Cryogenic Transmission Electron Microscopy	5
1.4. Small Angle Neutron Scattering.....	6
Spherical Form Factor	8
Spherical Core-Shell Form Factor	8
Ellipsoidal Core-Shell Form Factor.....	8
Lorentzian Function	9
Fractal Structure Factor	9
Cylinder Form Factor	10
Cylindrical Core-Shell Form Factor.....	10
2. Results and Discussion.....	11
2.1. Structure Freezing by Dilution	11
DLS Results.....	11
SANS Results	15
Cryo-TEM Results	17
Structural Parameters of Kinetically Frozen IPEC Micelles	21
2.2. Structure Freezing by Dialysis	22
DLS Results.....	22
SANS Results	23
2.3. Interpolyelectrolyte Complexation without Salt.....	27
DLS Results.....	27
SANS Results	28
2.4. Concentrated Equilibrated IPEC Solution.....	31
2.5. Comparative Discussion.....	32
3. References	36

1. Experimental Procedures

1.1. Sample Preparation

The interpolyelectrolyte complexes (IPECs) formed in aqueous mixtures of the used polymers have been analyzed concerning their quasi-equilibrium micellar structure in aqueous 0.3 M NaCl solution and the kinetics of complex formation towards equilibrium before.^{1,2} The miktoarm star polymer poly(ethylene oxide)₁₁₄-(poly([2-(methacryloyloxy)ethyl] trimethylammonium iodide)₁₇)₄ was synthesized according to procedures described in Ref. 3. The diblock copolymer poly(lithium vinylsulfonate)₃₁-*b*-poly(*N*-isopropyl acrylamide)₂₇ was synthesized as described in Ref. 4. For simplicity, the polymers will be labeled with STAR and DIBLOCK in the following text. Sodium chloride (NaCl, 99.8 %) was purchased from VWR. Deuterium oxide (D₂O, 99.95 %) was used as the solvent and obtained from Deutero.

The nomenclature of the samples (Scheme S1) contains specifications of the preparation temperature (pt) and the measurement temperature (mt), which are either 20 °C or 60 °C and will be given as, e.g., pt20 or mt60. IPEC-dialyzed-pt20-mt60, e.g., describes a sample that was kinetically frozen by eliminating the NaCl by dialysis at 20 °C (pt20) and afterwards was heated to 60 °C (mt60) to characterize the resulting assemblies above the lower critical solution temperature (LCST) of PNIPAM. As a second example IPEC-frozen-pt60-mt20 was prepared (equilibrated and diluted) at 60 °C, cooled below the LCST and characterized at 20 °C. For the preparation at 60 °C, all materials used (beakers, solvent, stock solutions etc.) were tempered beforehand at 60 °C. For the preparation of the IPEC samples a consistent mixing sequence was applied: the DIBLOCK solution was added first and the STAR solution second.

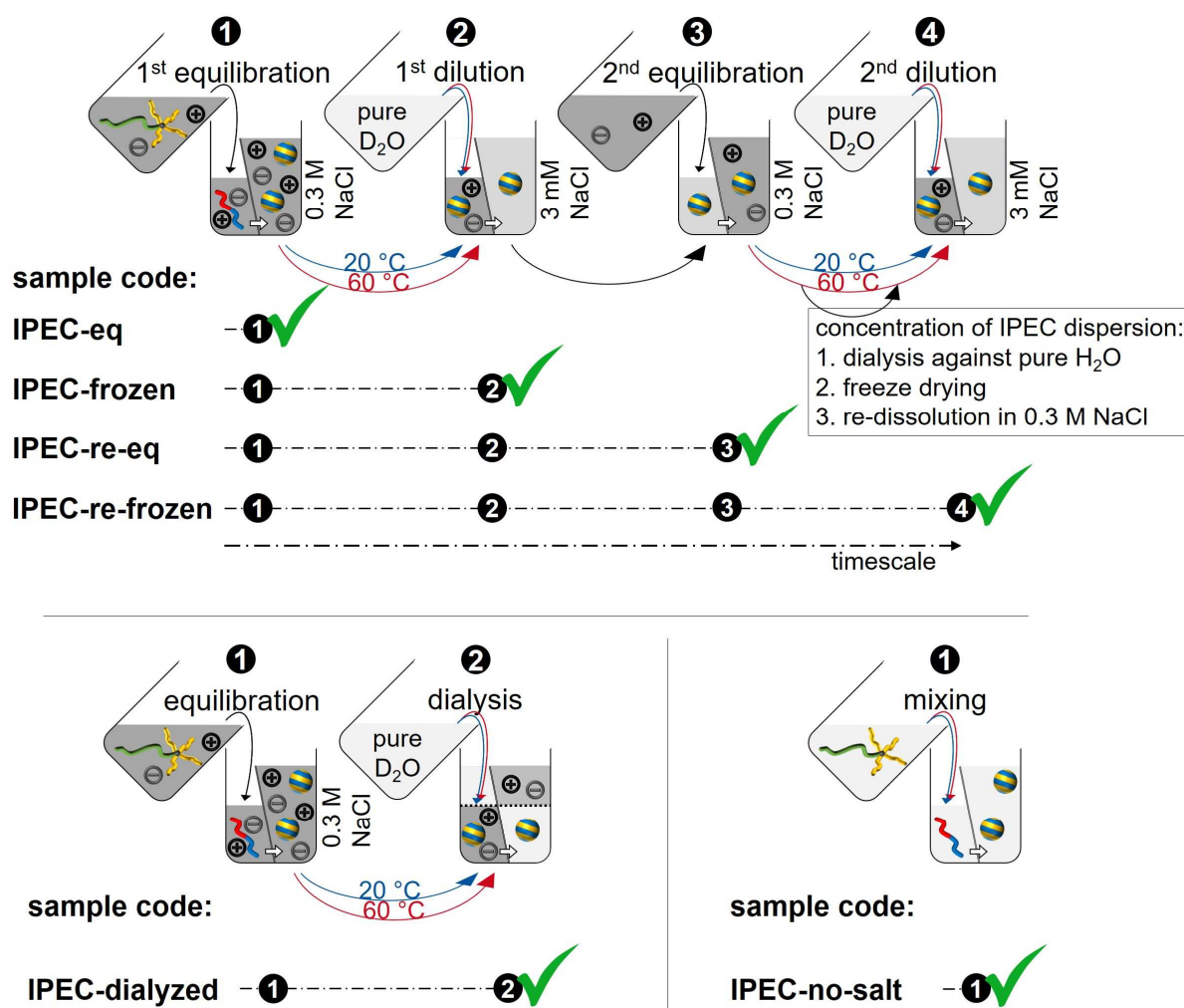
The IPEC samples discussed in the main part were prepared according to the following procedure: Stock solutions of STAR and DIBLOCK were prepared in D₂O, containing 0.3 M NaCl. The concentration of charged groups of the polyelectrolytes was 0.4 M for both stock solutions. Concentrated IPEC solutions were prepared by adding the STAR to the DIBLOCK stock solution. Before further treatment, the concentrated polymer solutions were equilibrated at room temperature or 60 °C for at least 24 h. A defined portion of the equilibrated IPEC solution was transferred to a vial and rapidly diluted (1:100 v/v) by addition of D₂O resulting in IPEC solutions with charge concentrations (positive and negative each) of 0.002 M and an overall polymer concentration of 0.09 wt%. Concentrated IPEC samples will be labelled with IPEC-eq and diluted samples with IPEC-frozen.

Alternatively, the salt content of the IPEC samples was reduced by dialysis. For this approach, stock solutions of STAR and DIBLOCK were prepared in D₂O (with 0.3 M NaCl) exhibiting concentrations of charged groups of 0.06 M. IPEC solutions were then prepared by mixing a 0.3 M NaCl solution with stock solutions of DIBLOCK and STAR resulting in an overall polymer concentration of 0.62 wt% (concentration of charged groups of 0.012 M each). After 3 d of equilibration at their preparation temperature, the solutions were transferred to dialysis capsules and dialyzed against D₂O (MWCO 1000 Da). The dialysis medium was exchanged two times after 1 d each time. After 3 d the dialysis was terminated and the solutions were transferred to vials. Dialyzed IPEC samples will be labelled with IPEC-dialyzed.

As a further reference system, IPEC samples were prepared without the addition of salt. For this purpose, stock solutions of STAR and DIBLOCK were prepared in D₂O with charge concentrations of 0.024 M. After mixing both stock solutions the samples IPEC-no-salt with an overall polymer concentration of

0.65 wt% and with concentrations of charged groups of each polymeric component of 0.012 M were stored at their preparation temperature for at least 24 h before measurement.

In order to verify the reversibility of the structure freezing process by dilution, a concentrated NaCl solution (3.27 M) was added to the IPEC-frozen samples resulting in a polymer concentration of 0.082 wt% and 0.3 M NaCl. The change in hydrodynamic size was investigated by use of DLS measurements. Furthermore, this re-equilibrated sample IPEC-re-eq-pt60 was dialyzed against bidistilled water to remove the salt. After freeze drying it was re-dissolved in a small amount of 0.3 M NaCl (D₂O) and the concentrated IPEC solution was equilibrated at 60 °C for 44 h. After dilution (1:100 v/v) with D₂O, resulting in a polymer concentration of about 0.09 wt%, the hydrodynamic size of the obtained frozen assemblies IPEC-re-frozen-pt60 was determined with DLS.



Scheme S1. Sample nomenclature and preparation history.

1.2. Dynamic Light Scattering

Dynamic light scattering experiments were performed on an ALV setup equipped with a goniometer (ALV, CGS-8F), a digital hardware correlator (ALV 5000), and a HeNe laser (JDS Uniphase, 35 mW) with a wavelength of $\lambda = 633$ nm. The samples were transferred to sealed cylindrical scattering cells and

placed in an index-match bath filled with toluene. The temperature was controlled with an external programmable thermostat (Julabo F32). The measurements were performed at scattering angles θ from 30 to 150° in increments of 10-20° and at temperatures from 20 to 60 °C in increments of 4 K. The CONTIN algorithm was applied to obtain the decay time distribution from the measured autocorrelation functions. The distributions were mainly bimodal as depicted in Figure S1. The largest species is assigned to loose aggregates and clusters.¹ The smaller species is identified as IPEC with micellar structure and thus as object of interest, though different coexisting micellar structures like fractal aggregates/worm-like micelles and vesicles can hardly be resolved in the DLS size distributions. The decay rates of these objects (roughly within the size range of 10-100 nm) were plotted against q^2 (with the scattering vector $q = (4\pi n/\lambda) \cdot \sin(\theta/2)$ with n as refractive index of the solution) to determine the z-average translational diffusion coefficient D_z of the scattering species. The average hydrodynamic radius R_h was calculated from D_z according to the Stokes-Einstein equation.

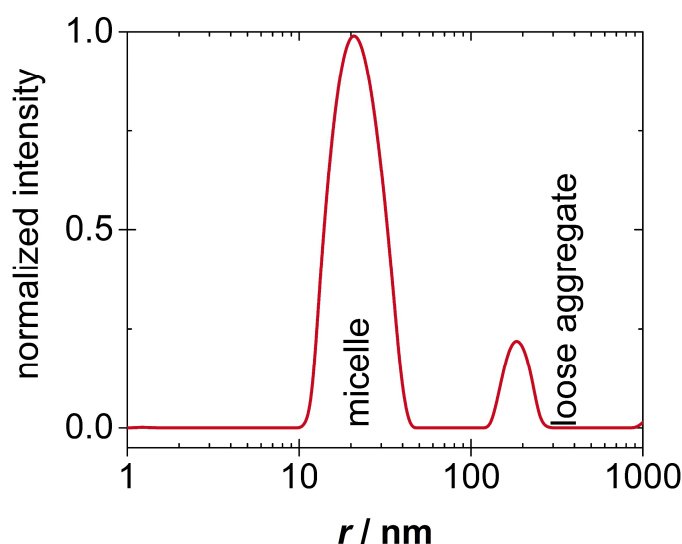


Figure S1. Example for an intensity-weighted CONTIN plot of the IPEC formed by STAR and DIBLOCK in aqueous solution showing a bimodal distribution according to micellar IPECs and loose aggregates (sample: IPEC-frozen-pt60-mt60 at 0.003 M NaCl, $\theta = 120^\circ$).

1.3. Cryogenic Transmission Electron Microscopy

For cryo-TEM studies, a sample droplet of 2 μ l (with total concentration of polymers 0.09 wt%) was put on a lacey carbon filmed copper grid (Science Services, München, Germany), which was hydrophilized by air plasma glow discharge (30 s with 10W, Solarus 950, Gatan, München, Germany). Subsequently, most of the liquid was removed with blotting paper leaving a thin film stretched over the lace holes. The specimens were instantly shock frozen by rapid immersion into liquid ethane cooled to approximately 90 K by liquid nitrogen in a temperature-controlled freezing unit (Leica EM GP, Leica Microsystems, GmbH, Wetzlar, Germany). The temperatures of 20 °C and 60 °C were monitored and kept constant in the chamber during all sample preparation steps. The specimen was inserted into a cryo-transfer holder (CT3500, Gatan, München, Germany) and transferred to a Zeiss/LEO EM922 Omega EFTEM (Zeiss Microscopy GmbH, Jena, Germany). Examinations were carried out at temperatures around 90 K. The TEM was operated at an acceleration voltage of 200 kV. Zero-loss filtered images

($\Delta E = 0$ eV) were taken under reduced dose conditions (100–1000 e nm⁻²). All images were registered digitally by a bottom mounted CCD camera system (Ultrascan 1000, Gatan, München, Germany) combined and processed with a digital imaging processing system (Digital Micrograph GMS 1.9, Gatan, München, Germany).

Cryo-TEM studies on the sample IPEC-re-frozen-pt60 were performed likewise. One drop of the sample was placed onto a hydrophilized carboncoated copper grid. The excessive solution was removed in a vitrobot system. The sample was vitrified from the aqueous dispersion by rapid introduction of the grid in liquid ethane. A Carl Zeiss LIBRA 120 microscope operating at 120 kV with a bottom mounted CCD camera was used to record the zero-loss energy-filtered transmission electron micrographs.

ImageJ software was used to analyze the images and to measure manually the size of the particles.⁵

1.4. Small Angle Neutron Scattering

Small angle neutron scattering (SANS) experiments were performed at the KWS-2 instrument at FRM II in Garching (Munich, Germany).⁶ Incident neutron wavelengths of 5 Å at detector distances of 2 and 8 m and 10 Å at 20 m were used, yielding a q -range of 0.002 to 0.474 Å⁻¹, as $q = (4\pi/\lambda) \sin \theta/2$ where λ is the wavelength and θ the scattering angle. The samples were prepared in deuterium oxide (D₂O) to provide good neutron scattering contrast. Samples were transferred to Hellma quartz glass cuvettes with pathlengths of 1 or 2 mm at room temperature or in the oven at 60 °C. Each sample was measured at 20 °C as well as at 60 °C. A calibrated thermostat was applied to reach temperatures of 20 and 60 °C within the sample cuvettes. The scattered intensity was collected on a 2D detector with an active area equivalent to 0.9 m².⁶ Each raw scattering data set was corrected for detector sensitivity, electronics background and sample transmission and converted to scattering cross-section data using instrument software QtiKWS. This data was converted to the absolute scale (cm⁻¹) through reference to the scattering from a secondary standard sample (Plexiglas).

The 1D scattering patterns were qualitatively and quantitatively analyzed with SasView 4.1.⁷ Form factor models (see below) implemented in SasView were fitted to the scattering data in appropriate q ranges. Additionally, particle distance distribution functions (PDDFs) $p(r)$ were calculated via inverse Fourier transformations (IFT) of the scattering data with SasView. The PDDFs depict the probability to find two points within a certain distance r within a particle.

For the description of the experimental scattering curves by form factor fitting the start values for the micellar sizes (radii, thicknesses etc.) were estimated on the basis of the PDDFs, the DLS data, cryo-TEM results and previous (published) form factor fits. The scattering length densities of the micellar domains were adjusted within certain limits. For this, scattering length densities of the pure components were estimated first (Table S1). Second, limits for the hydration of these domains (volume fraction of D₂O ϕ_{D_2O}) were assumed (Table S2). Finally, it was possible to define the limits for the domain SLDs ρ_{domain} according to the following formula: $\rho_{\text{domain}} = \phi_i \cdot \rho_i + (1 - \phi_i) \cdot \rho_{D_2O}$ with ρ_i and ϕ_i as SLD and volume fraction of the pure components, respectively, and ρ_{D_2O} as SLD of the solvent (Table S2). As start value used for form factor fitting, an average SLD was used for the single domains, which could adjust freely within the determined limits (Table S3). The scattering length densities of hydrated PEO and PNIPAM are rather similar, so it is hardly possible to resolve a compartmentalization in the corona structure at 20 °C. Thus, no further domains are distinguished within the corona. For the partly dehydrated PNIPAM at temperatures above its LCST, the possible SLDs are in the range of the SLD

limits assumed for the IPEC domain (Table S2). Consequently, it is also not possible to describe the compartmentalization of the core structure at 60 °C by our SANS data analysis.

Table S1. Estimated scattering length densities (SLD) ρ for D₂O and the pure polymer compounds calculated with SasView software.

component	SLD [10^{-6} \AA^{-2}]
D ₂ O	6.39
PEO	0.64
PNIPAM	0.81
PEO+PNIPAM	0.73
<i>q</i> PDMAEMA	0.62
PVS	1.59
IPEC	1.00

Table S2. Supposed degree of hydration of different micellar domains and consequent limits for the SLDs of these domains.

micelle domain	$\phi_{\text{D}_2\text{O}}$	SLD [10^{-6} \AA^{-2}]
corona (PEO, PEO+PNIPAM)	0.7 – 0.95	4.69 – 6.11
PNIPAM at $T > \text{LCST}$	0.5 – 0.6	3.60 – 4.16
IPEC	0.3 – 0.7	2.62 – 4.77

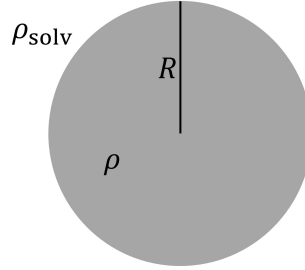
Table S3. Start values of the domain SLDs and corresponding limits for the form factor fitting process.

micelle domain	start value SLD [10^{-6} \AA^{-2}]	limits SLD [10^{-6} \AA^{-2}]
corona (20 and 60 °C)	5.4	4.69 – 6.11
IPEC (20 °C) or IPEC+PNIPAM (60 °C)	3.7	2.62 – 4.77
PEO+PNIPAM+IPEC (20 and 60 °C)	4.5	2.62 – 6.11

In order to model the entire scattering curve, combined form factor fits were used. The strongly increasing intensity toward low q values is indicative of aggregates. For simplicity, these aggregates were described as simple monodisperse spheres. The adjustment of the form factor fits at low q values is therefore only of moderate quality, but gives an approximation for the size of loose aggregates. Toward the high q limit, the scattering intensities often decrease slowly. Here, the scattering contribution might arise from interaction between single chains, so entanglements. In some cases, this region is well described by a Lorentz function that gives a correlation length ζ , which is large for highly correlated systems. The mid- q region mainly results from the scattering of the micellar IPECs, which are of interest for us. For the description of this q region, more detailed form factor models were applied including either a sum of two simple form factors, modelling the overall shape of coexisting species, or single complex form factors, which allow conclusions on the inner structure of the micellar IPECs. In general, it was tried to keep the models applied in form factor fitting as simple as possible to obtain reliable information from SANS data analysis without over-parameterization. In this sense, also the polydispersity σ is disregarded and set to 0, e.g., in case of the radius of spherical aggregates or the length of cylindrical micelles. All applied form factor models are described in the following.

Spherical Form Factor

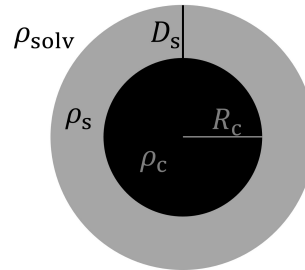
$$I(q) = \frac{scale}{V} \cdot \left[3V(\rho - \rho_{solv}) \cdot \frac{\sin(qR) - qR \cos(qR)}{(qR)^3} \right]^2 + bkg. \quad ^8$$



- scale*: scale factor
V: volume of scatterer
ρ: scattering length density of scatterer
ρ_{solv}: scattering length density of the solvent
R: radius of the sphere
bkg: background scattering

Spherical Core-Shell Form Factor

$$P_{cs-sphere}(q) = \frac{scale}{V_s} \left[3V_c(\rho_c - \rho_s) \frac{[\sin(qR_c) - qR_c \cos(qR_c)]}{(qR_c)^3} + 3V_s(\rho_s - \rho_{solv}) \frac{[\sin(qD_s) - qD_s \cos(qD_s)]}{(qD_s)^3} \right]^2 + bkg. \quad ^8$$



- scale*: scale factor
V_s: volume of the outer shell
V_c: volume of the core
ρ_c: scattering length density of the core (equal to ρ_{solv} for hollow spheres)
ρ_s: scattering length density of the shell
ρ_{solv}: scattering length density of the solvent
R_c: radius of the core
D_s: thickness of the shell
bkg: background scattering

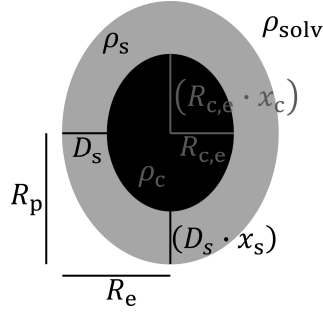
Ellipsoidal Core-Shell Form Factor

$$P(q, \alpha) = \frac{scale}{V} F^2(q, \alpha) + bkg. \quad ^9$$

$$F(q, \alpha) = f(q, R_{c,e}, R_{c,e} \cdot x_c, \alpha) + f(q, R_{c,e} + D_s, R_{c,e} \cdot x_c + D_s \cdot x_s, \alpha)$$

$$f(q, R_e, R_p, \alpha) = \frac{3\Delta\rho V(\sin[qr(R_e, R_p, \alpha)] - \cos[qr(R_e, R_p, \alpha)])}{[qr(R_e, R_p, \alpha)]^3}$$

$$r(R_e, R_p, \alpha) = [R_e^2 \sin^2 \alpha + R_p^2 \cos^2 \alpha]^{1/2}$$



- scale*: scale factor
V: volume of the ellipsoid
R_e: equatorial radius
R_p: polar radius
R_{c,e}: equatorial radius of core
x_c: axial ratio of core (pole to equator)
D_s: thickness of shell at equator
x_s: ratio of thickness of shell (pole to equator)
 $\Delta\rho$: contrast: $(\rho_c - \rho_s)$ or $(\rho_s - \rho_{solv})$
 ρ_c : scattering length density of the core
 ρ_s : scattering length density of the shell
 ρ_{solv} : scattering length density of the solvent
 α : angle between the axis of the ellipsoid and *q*
bkg: background scattering

Lorentzian Function

$$I(q) = \frac{scale}{1+(q\xi)^2} + bkg. \quad ^{10}$$

- scale*: scale factor
 ξ : screening / correlation length
bkg: background scattering

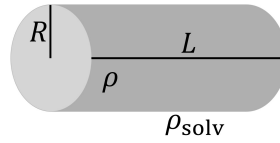
Fractal Structure Factor

$$S_{fractal}(q) = 1 + \frac{D_f \Gamma(D_f - 1) \sin((D_f - 1) \tan^{-1}(q\xi))}{(qR)^{D_f} \left(1 + \frac{1}{q^2 \xi^2}\right)^{\frac{D_f - 1}{2}}}. \quad ^{11}$$

D_f : fractal dimension
 Γ : gamma function
 ξ : correlation length
 R : radius of the particle

Cylinder Form Factor

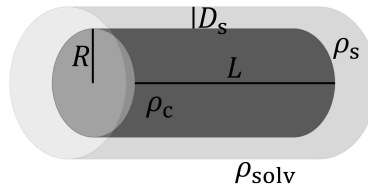
$$P_{\text{cylinder}}(q, \alpha) = \frac{\text{scale}}{V} \left[2V(\rho - \rho_{\text{solv}}) \frac{\sin\left(\frac{1}{2}qL \cos \alpha\right)}{\frac{1}{2}qL \cos \alpha} \frac{J_1(qR \sin \alpha)}{qR \sin \alpha} \right]^2 + bkg. \quad 8$$



scale : scale factor
 V : volume of the cylinder
 ρ : scattering length density of the cylinder
 ρ_{solv} : scattering length density of the solvent
 L : length of the cylinder
 R : radius of the cylinder
 α : angle between the axis of the cylinder and the q -vector
 J_1 : first order Bessel function of the first kind
 bkg : background scattering

Cylindrical Core-Shell Form Factor

$$P_{\text{cs-cylinder}}(q, \alpha) = \frac{\text{scale}}{V} \left[2V_c(\rho_c - \rho_s) \frac{\sin\left(\frac{1}{2}qL \cos \alpha\right)}{\frac{1}{2}qL \cos \alpha} \frac{J_1(qR_c \sin \alpha)}{qR_c \sin \alpha} + 2V(\rho_s - \rho_{\text{solv}}) \frac{\sin\left(\frac{1}{2}q(L+2D_s) \cos \alpha\right)}{\frac{1}{2}q(L+2D_s) \cos \alpha} \frac{J_1(q(R_c+D_s) \sin \alpha)}{q(R_c+D_s) \sin \alpha} \right]^2 + bkg. \quad 12$$



scale : scale factor
 V : volume of the cylinder $V = \pi(R_c + D_s)^2(L + 2D_s)$
 V_c : volume of the core
 ρ_c : scattering length density of the core
 ρ_s : scattering length density of the shell
 ρ_{solv} : scattering length density of the solvent
 L : length of the core
 R_c : radius of the core

D_s :	thickness of the shell
α :	angle between the axis of the cylinder and the q -vector
J_1 :	first order Bessel function of the first kind
bkg :	background scattering

2. Results and Discussion

2.1. Structure Freezing by Dilution

DLS Results

The intermediate scattering function derived from DLS measurements is the sum of exponential decays resulting from different types of motion. For monodisperse rigid rods of length L Pecora stated that for $qL < 5$ (with the amount of the scattering vector q) only the translational motion of the particles contributes discernibly to the total scattered intensity.¹³ Hence, the intermediate scattering function contains only one exponential decay. For $qL > 5$ a second exponential decay must be considered, which is related to the rotational diffusion.¹³ Cryo-TEM images obtained for IPEC-frozen-pt60-mt20 show worm-like structures with a length of about 91 nm (Figure 3D). Thus, according to Pecora the scattered intensity derived in the investigated angular range (30° - 150°) should solely result from translational diffusion here. Apart from this, in general it is unusual to find a depolarized mode for polymeric samples. Although it is not expected from the previous explanations, the decay rate of IPEC-frozen-pt60 shows y-intercepts different from 0 at 20 as well as at 60 °C (red dashed and solid lines in Figure S2). This might be an indication for additional relaxation processes (rotational diffusion) as expected, e.g., for elongated particles.

Tirado and Garcia de la Torre established an expression for the diffusion coefficient of rigid rods: $D_T = (kT/3\pi\eta L)(\ln p + 0.312 + 0.565/p - 0.1/p^2)$.¹⁴⁻¹⁵ The parameter p is the ratio of rod length L and rod diameter d . Cryo-TEM images obtained for IPEC-frozen-pt60-mt20 (Figure 3D) show worm-like structures with a diameter of about 11 nm and a length of about 91 nm (Table S5). If these values are plugged in the equation, a translational diffusion coefficient D_T of $9.52 \cdot 10^{-12} \text{ m}^2\text{s}^{-1}$ is calculated, which is almost equal to the experimentally obtained diffusion coefficient from DLS analysis ($9.57 \cdot 10^{-12} \text{ m}^2\text{s}^{-1}$). As the objects visible in cryo-TEM images probably might not (fully) contain the water-soluble PEO and PNIPAM corona (see discussion below), the above-mentioned equation can be used to calculate the rod length under assumption of a bigger diameter and use of the experimental D_T : For a diameter of 15 nm a rod length of 73 nm and for $d = 20$ nm a length of 55 nm is obtained. The model of Tirado and Garcia de la Torre is valid for rigid rods. The cryo-TEM images in Figure 3D, however, show bent and possibly flexible worm-like structures. Thus, the above equation has only limited validity here, but can be considered as good approximation. Consequently, the DLS data of IPEC-frozen-pt60 correspond very well with the results obtained from SANS and cryo-TEM data analysis.

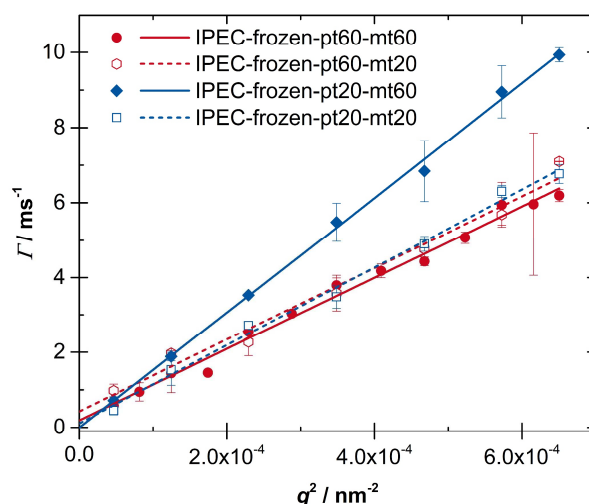


Figure S2. Decay rate Γ obtained by CONTIN analysis of DLS results of IPEC micelles kinetically frozen by dilution after equilibration in 0.3 M NaCl (D_2O) plotted versus q^2 .

With DLS measurements it is further possible to examine the stability of the kinetically frozen IPEC assemblies. Due to the huge size difference to the equilibrated state at 60 °C the sample IPEC-frozen-pt60 was chosen for this experiment. 27 days after the first DLS study (the results of this is presented in Figure 1, Figure S2 and in Figure S3 as solid lines) a second set of measurements was performed with the physically same sample IPEC-frozen-pt60. As depicted in Figure S3 the same sizes, within the range of error, were determined for both measurements at 20 °C as well as at 60 °C. Figure S3 further shows that the different kinetically frozen assemblies below and above the LCST of PNIPAM are repeatedly rearranged into each other by heating and cooling. Hence, these DLS studies prove the stability of the kinetically frozen IPEC micelles as well as the reversibility of their size (and structure) change upon varying the temperature around the LCST.

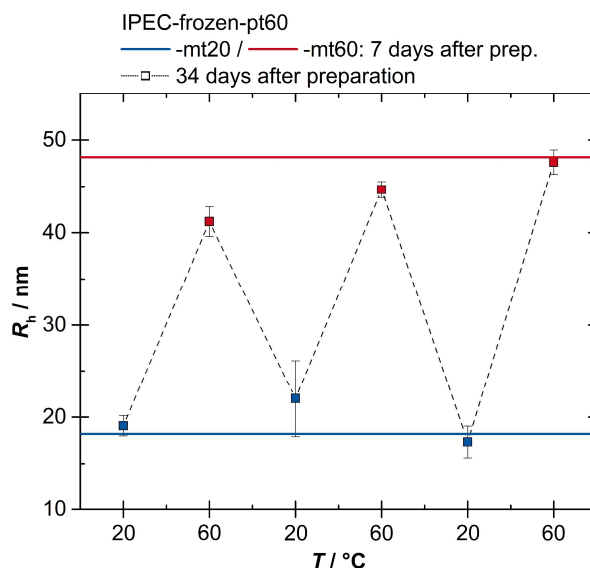


Figure S3. The hydrodynamic radius R_h of kinetically frozen IPEC micelles (IPEC-frozen-pt60) measured at 20 °C and 60 °C and at different times after preparation (solid lines: 7 days after preparation, squares: 34 days after preparation). The polymer concentration is ~ 0.09 wt% for diluted systems. The dashed lines are guides to the eyes only.

The identification and structural analysis of intermediate micellar structures at temperatures near the LCST of PNIPAM is challenging. Hence, it is hardly possible to differentiate intermediately formed IPEC assemblies when crossing the LCST upon heating or cooling. A first impression on the restructuring processes at the transition temperature upon heating and cooling might, however, be obtained from the hydrodynamic sizes. Figure S4B depicts the heating curve for the sample IPEC-frozen prepared at 60 °C in red (cf. also Figure 1) and a cooling curve for the same sample in black. Within the range of error, the R_h is the same for the heating and cooling curve for temperatures below and above the LCST. Thus, for the investigated temperature intervals no hysteresis is observed. However, close to the transition at 36 °C just one species was found for the heating process by DLS. This might indicate that the aggregation of PNIPAM blocks results in the formation of assemblies with an increased aggregation number within one step. In contrast, for the cooling process two species of distinctly different sizes were found. The R_h of the main species is similar to that of the heating cycle, whereas the radius of the minor species is right in between those obtained at 20 and 60 °C. Hence, upon resolubilization of the PNIPAM blocks some intermediate structures might be obtained during the vesicle-to-worm transition.¹⁶ A similar scenario is observed for IPEC-frozen-pt20 as depicted in Figure S4A.

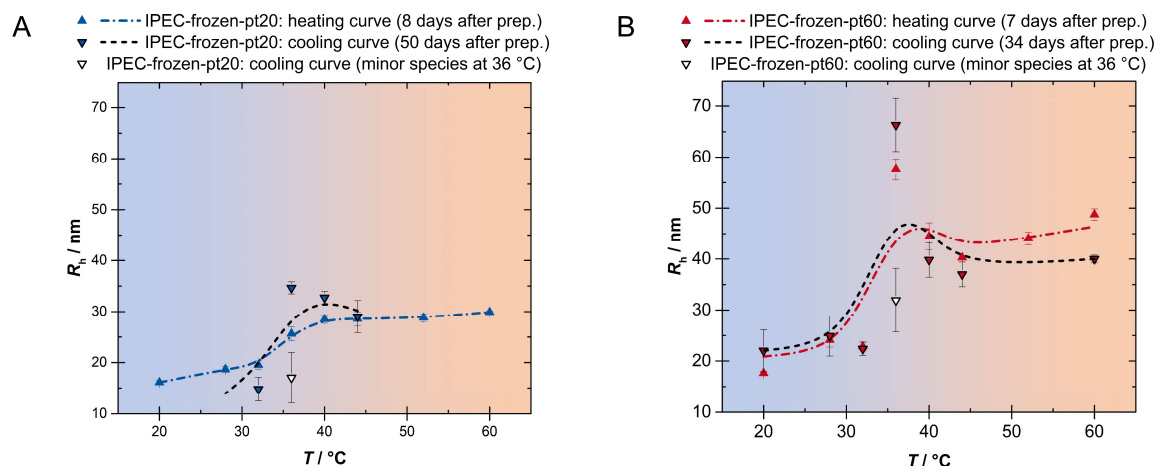


Figure S4. Temperature dependence of the R_h of IPEC micelles upon heating from 20 °C to 60 °C (colored symbols and lines) and cooling (black symbols and lines) measured by DLS for different preparation temperatures (pt) of 20 °C (A) and 60 °C (B). The polymer concentration is ~ 0.09 wt% for diluted systems. The dashed lines are guides to the eyes only.

In comparison to the equilibrated micellar IPECs, the assemblies kinetically frozen by dilution exhibit larger radii and/or different structures.¹ When the NaCl content in IPEC-frozen-pt60 is adjusted to 0.3 M, the hydrodynamic radius of the micellar IPECs is decreased (cf. yellow filled hexagon in Figure 1 and Figure S5) approaching the values determined for the equilibrated sample (black filled hexagon). This indicates that the addition of salt leads to a rather rapid rearrangement of the IPECs towards the equilibrium micellar structures. This process might be reversed by removing the added salt via dialysis. After freeze-drying the IPEC, a concentrated polymer solution (IPEC-re-eq) is prepared in 0.3 M NaCl, which is diluted (1:100 v/v) with D₂O after equilibration at 60 °C (IPEC-re-frozen-pt60). The micellar IPECs now exhibit the same hydrodynamic radius as was obtained after the first dilution approach proving full reversibility of the generation of nonequilibrium structures (cf. red circle filled yellow in Figure 1 and Figure S5). This result further suggests that the freeze-drying process does not affect the IPEC. Addition of salt to IPEC-frozen-pt20, however, does not result in a decrease of the R_h below the LCST (cf. blue filled grey diamond in Figure S5). A rearrangement does not occur as the kinetically frozen and the equilibrated structure are basically identical. At temperatures above the LCST the radius is slightly reduced presumably indicating that now core-shell-shell spheres or worms are formed rather than vesicles.

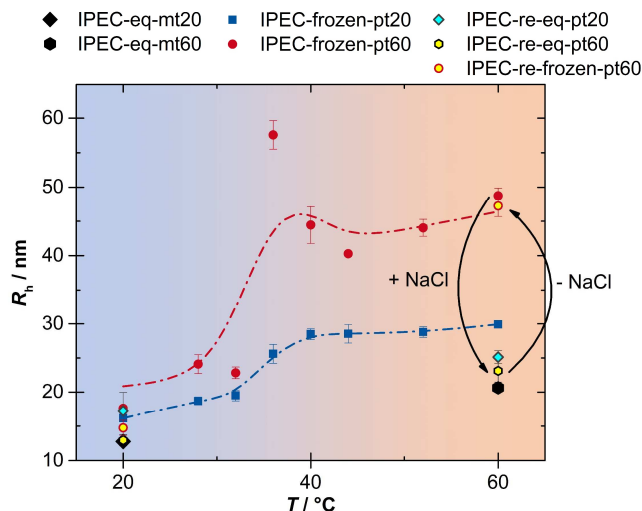


Figure S5. Temperature dependence of the R_h of IPEC micelles upon heating from 20 °C to 60 °C measured by DLS for different preparation temperatures (pt). The polymer concentration is ~ 0.09 wt% for diluted systems. The dashed lines are guides to the eyes only.

SANS Results

For the micellar IPEC assemblies, which were kinetically frozen by dilution, form factor fits were conducted for the whole q range as presented in the main part (Figure 2). PDDFs were calculated for $q > 0.005 \text{ \AA}^{-1}$ to neglect the scattering contribution of loose aggregates. As Figure S6 shows, distinctly different distribution functions are obtained for the investigated q -range at a measurement temperature of 20 °C. From these it might be deduced that elongated structures are present for a preparation temperature of 60 °C, whereas spherical-like assemblies have formed upon equilibration and dilution at room temperature. These results are in line with the form factor fits presented in the main part and in Table S4.

For measurements at temperatures above the LCST of PNIPAM (Figure S6B), the PDDFs suggest the existence of micelles with a spherical to slightly elongated shape in case of a preparation at $T < \text{LCST}$. This possibly results from the small fractal aggregates visible in the cryo-TEM images described in the main part. Besides of the fractal aggregates also vesicular structures were observed in cryo-TEM analysis. For the sample prepared at 60 °C, the PDDF also suggests the formation of elongated species rather than vesicles. Due to the coexistence of different structures, it is hard to draw detailed conclusions from the PDDFs at high measurement temperature. Therefore, the cryo-TEM images were used as an aid to find appropriate form factor models for SANS data fitting.

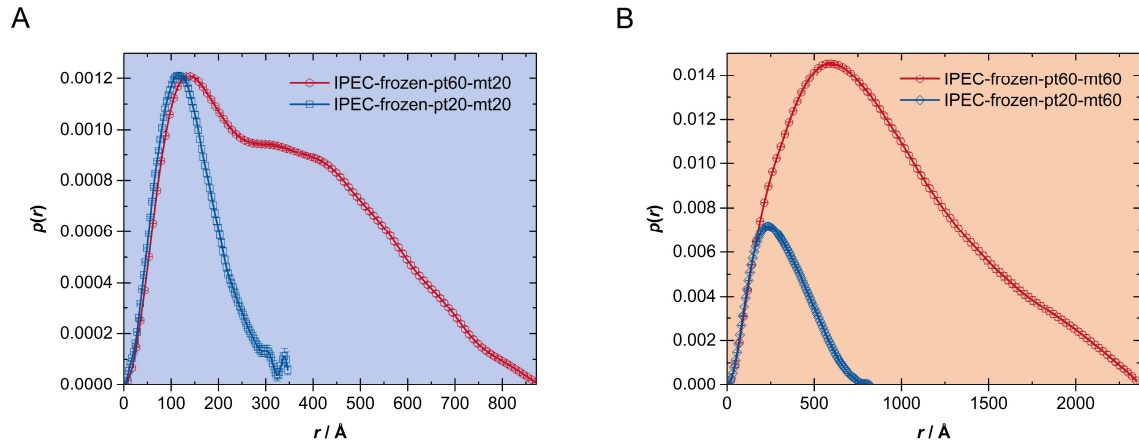
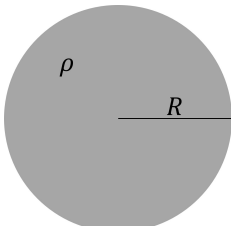
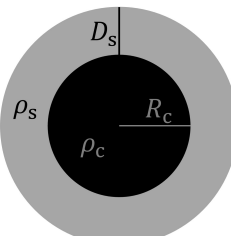
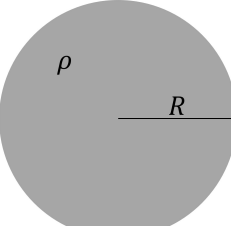
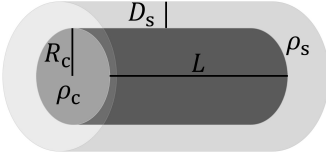
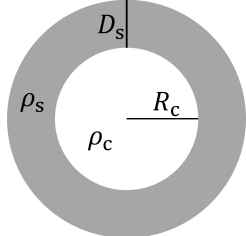
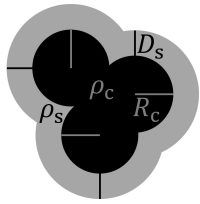
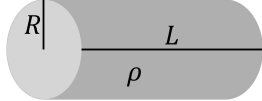
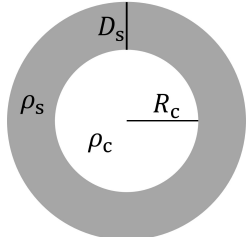


Figure S6. PDDFs calculated via IFT from the scattering data of IPEC-frozen measured at 20 °C (A) and 60 °C (B).

Table S4. Structural parameters of kinetically frozen IPEC micelles prepared at different temperatures (20 °C and 60 °C), diluted and measured at different temperatures obtained from SANS data analysis. The corresponding SANS data and form factor fits are presented in Figure 2.

sample	form factor model	fit results
IPEC-frozen -pt20-mt20		spherical aggregate: $R = 140.0 \text{ nm}$ (σ set to 0) $\rho = 5.9 \cdot 10^{-6} \text{ \AA}^{-1}$
		spherical core-shell micelle: $R_c = 6.8 \text{ nm}$ ($\sigma_c = 0.32$) $D_s = 4.7 \text{ nm}$ ($\sigma_s = 0.01$) $\rho_c = 4.1 \cdot 10^{-6} \text{ \AA}^{-1}$ $\rho_s = 5.4 \cdot 10^{-6} \text{ \AA}^{-1}$
		Lorentzian function: $\xi = 3.4 \text{ nm}$
IPEC-frozen -pt60-mt20		spherical aggregate: $R = 140.0 \text{ nm}$ (fixed) (σ set to 0) $\rho = 4.6 \cdot 10^{-6} \text{ \AA}^{-1}$

		cylindrical core-shell micelle: $R_c = 4.7 \text{ nm}$ ($\sigma_c = 0.33$) $D_s = 5.9 \text{ nm}$ ($\sigma_s = 0.42$) $L = 153.7 \text{ nm}$ (σ set to 0) $\rho_c = 4.0 \cdot 10^{-6} \text{ \AA}^{-1}$ $\rho_s = 5.9 \cdot 10^{-6} \text{ \AA}^{-1}$
		hollow sphere (vesicle): $R_c = 8.6 \text{ nm}$ ($\sigma_c = 0.23$) $D_s = 18.5 \text{ nm}$ ($\sigma_s = 0.12$) $\rho_c = 6.4 \cdot 10^{-6} \text{ \AA}^{-1}$ (fixed) $\rho_s = 4.8 \cdot 10^{-6} \text{ \AA}^{-1}$
IPEC-frozen -pt20-mt60		fractal aggregate from core-shell spheres: $R_c = 13.8 \text{ nm}$ ($\sigma_c = 0.30$) $D_s = 9.3 \text{ nm}$ ($\sigma_s = 0.03$) $\rho_c = 3.5 \cdot 10^{-6} \text{ \AA}^{-1}$ $\rho_s = 6.1 \cdot 10^{-6} \text{ \AA}^{-1}$ $D_f = 2.8$ $\xi = 19.3 \text{ nm}$
		cylindrical micelle: $R = 17.4 \text{ nm}$ ($\sigma = 0.50$) $L = 94.1 \text{ nm}$ (σ set to 0) $\rho = 4.8 \cdot 10^{-6} \text{ \AA}^{-1}$
IPEC-frozen -pt60-mt60		hollow sphere (vesicle): $R_c = 28.6 \text{ nm}$ ($\sigma_c = 0.78$) $D_s = 17.5 \text{ nm}$ ($\sigma_s = 0.01$) $\rho_c = 6.4 \cdot 10^{-6} \text{ \AA}^{-1}$ (fixed) $\rho_s = 3.7 \cdot 10^{-6} \text{ \AA}^{-1}$

pt: preparation temperature, mt: measurement temperature, R : radius, D : thickness, L : length, ξ : correlation length, ρ : scattering length density, σ : polydispersity, c: core, s: shell, D_f : fractal dimension.

Cryo-TEM Results

Cryo-TEM images of polymeric micelles kinetically frozen by dilution are presented in Figure 3 in the main part and in Figure S7. For IPEC-frozen-pt20-mt20 178 of these spherical-like micelles depicted in Figure 3A were evaluated yielding an average radius of $8.5 \pm 1.4 \text{ nm}$ for the dark grainy spots (Figure S8A). These mainly correspond to the IPEC domain itself which exhibits the highest electron density and thus is visible in cryo-TEM images. The mixed PEO-PNIPAM corona presumably just marginally contributes to the dimension of the observed objects. Thus, the radius is in good agreement with the core size obtained from SANS data fitting. Further it is consistent with the radial size of 8.7 nm found for the equilibrated IPEC sample at 20°C as stated elsewhere.¹

At temperatures above the LCST of PNIPAM, the spherical objects formed by equilibration and dilution at room temperature aggregate due to the collapse of the PNIPAM blocks. The cryo-TEM images presented in Figure 3B clearly show vesicular structures which seem to have an irregular membrane with localized dark spots. These darker parts, which are partly highlighted in Figure S7C, might depict the IPEC domains. It is conceivable that the spherical core structures present at 20 °C as described above are preserved upon heating as rearrangements are prevented in the absence of low molecular weight salt. The vesicles are therefore formed by aggregation of dehydrated PNIPAM blocks of different micelles, presumably depicted by the brighter parts of the membrane. 154 of these vesicular objects were analyzed concerning their size. The average radius including the membrane visible in cryo-TEM images is 34.7 ± 7.9 nm (Figure S8C). The membrane, presumably containing the IPEC domain as well as the collapsed PNIPAM blocks, exhibits an average thickness of 9.8 ± 2.3 nm (the thickness was determined from 56 vesicles at 10 positions for each object, Figure S8D). However, the spherical micelles are not completely consumed by vesicle formation, but further form some irregular spherical- or elongated-like aggregates with a loose inner structure (Figure 3B). Accordingly, the corresponding SANS data could be well described with a combination of form factors of a hollow core-shell sphere and a fractal structure with core-shell spheres as primary building blocks (Figure 2).

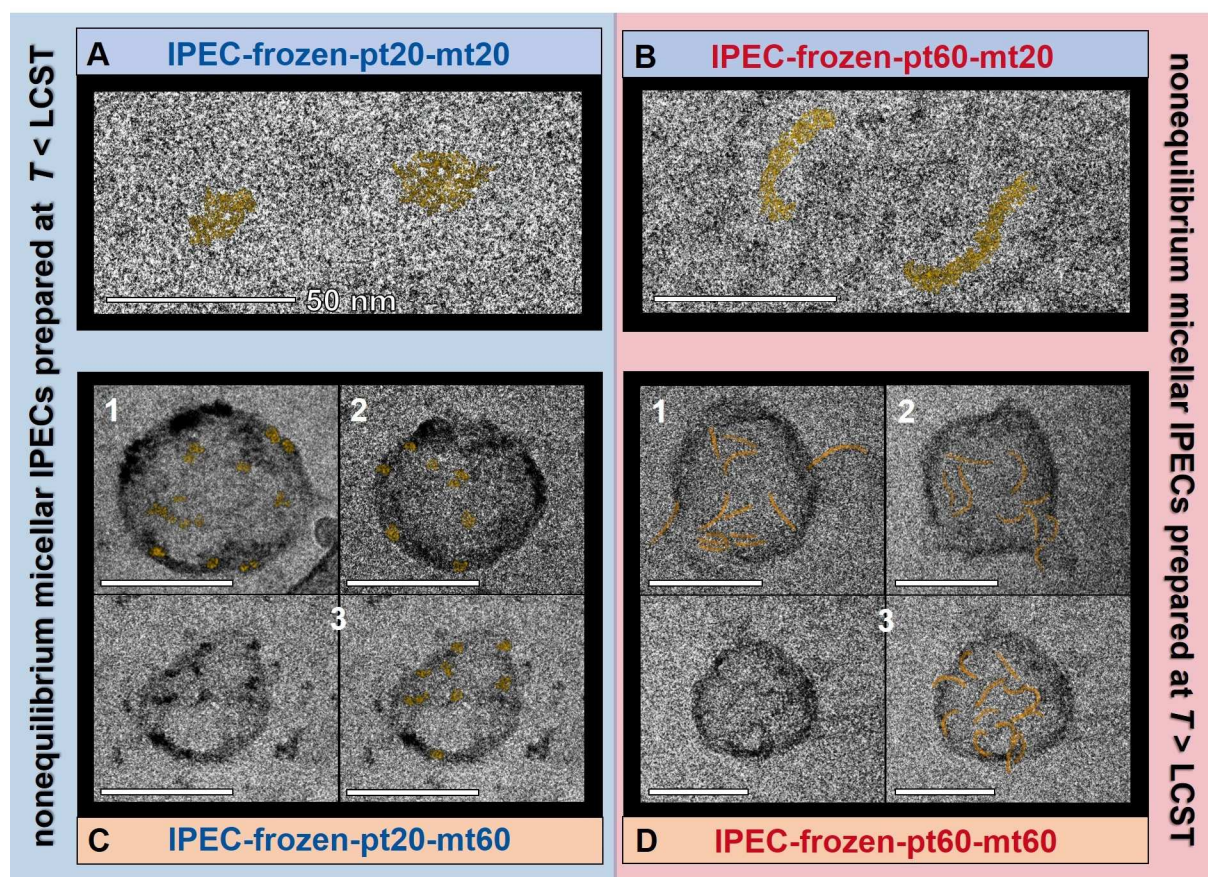


Figure S7. Cryo-TEM images of kinetically frozen IPEC micelles prepared at 20 °C (A, C) and 60 °C (B, D) and then shock vitrified at 20 °C (A, B) and 60 °C (C, D). The scale bars correspond to a length of 100 nm except where not otherwise stated. The yellow color exemplarily highlights some insoluble IPEC domains with its grainy substructure at 20 °C (A, B) and its spherical or worm-like shape in the vesicle membranes at 60 °C (C, D). For A, B, C1, C2, D1, D2 the original images are depicted in Figure 3.

The IPEC sample equilibrated and frozen at $T > \text{LCST}$ consists of elongated, partly branched micellar structures which can be seen in the background of the cryo-TEM images (partly marked in red in Figure 3C). The diameter of these observed worms seems to be similar to that determined at 20 °C (see below), which is surprising as it was expected that the collapsed PNIPAM blocks contribute to the thickness of the elongated core. Additionally, some vesicles which partly exhibit damages are observed in cryo-TEM images (Figure 3C). These seem to exhibit a rather uniform membrane as opposed to IPEC-frozen-pt20-mt60. It might be conceivable that these vesicles are built up from an aggregation of the bent worms, which are present at $T < \text{LCST}$. Such worm-like structures, which might be found on closer inspection, are highlighted in Figure S7D. 28 of these objects were analyzed concerning their size and membrane thickness (Figure S8E-F). The evaluation revealed that the vesicular structures exhibit a broader size distribution as those obtained from the sample prepared at room temperature. An average vesicle radius (including the visible membrane) of 68.2 ± 22.7 nm was determined with a membrane thickness of 11.8 ± 3.2 nm (the thickness was determined at 5 positions for each vesicular object). By help of this cryo-TEM analysis, the SANS data were well described with a sum of form factors describing a simple cylinder and a hollow core-shell sphere as indicated in Figure 2.

Cryo-TEM images of IPEC-frozen-pt60-mt20 clearly show bent worm-like objects, which also exhibit a grainy substructure (Figure 3D, highlighted in Figure S7B). This probably depicts the water-insoluble IPEC domain forming the elongated micellar core. 12 of these objects were investigated concerning their core diameter and length. The diameter of each worm was determined at 7 positions yielding an average thickness of 11.3 ± 2.1 nm (Figure S8B). This is approximately the same magnitude as obtained from SANS data fitting. Cryo-TEM images of a sample equilibrated and shock vitrified at 60 °C show worm-like structures with a core diameter of 18.3 nm.¹ These are bigger in size as apart from the IPEC domain the dehydrated and collapsed PNIPAM blocks are part of the water-insoluble core. Further, the investigated objects depicted in Figure 3D exhibit an average core length of 86 ± 21 nm.

The same structures are observed after repeating the freezing process at $T > \text{LCST}$ (Figure 3D). Cryo-TEM images of IPEC-re-frozen-pt60-mt20 show bent worm-like micelles of similar sizes as obtained after the first freezing cycle. Together with the DLS data this proves the fully reversible switching between well-defined equilibrium and nonequilibrium micellar assemblies.

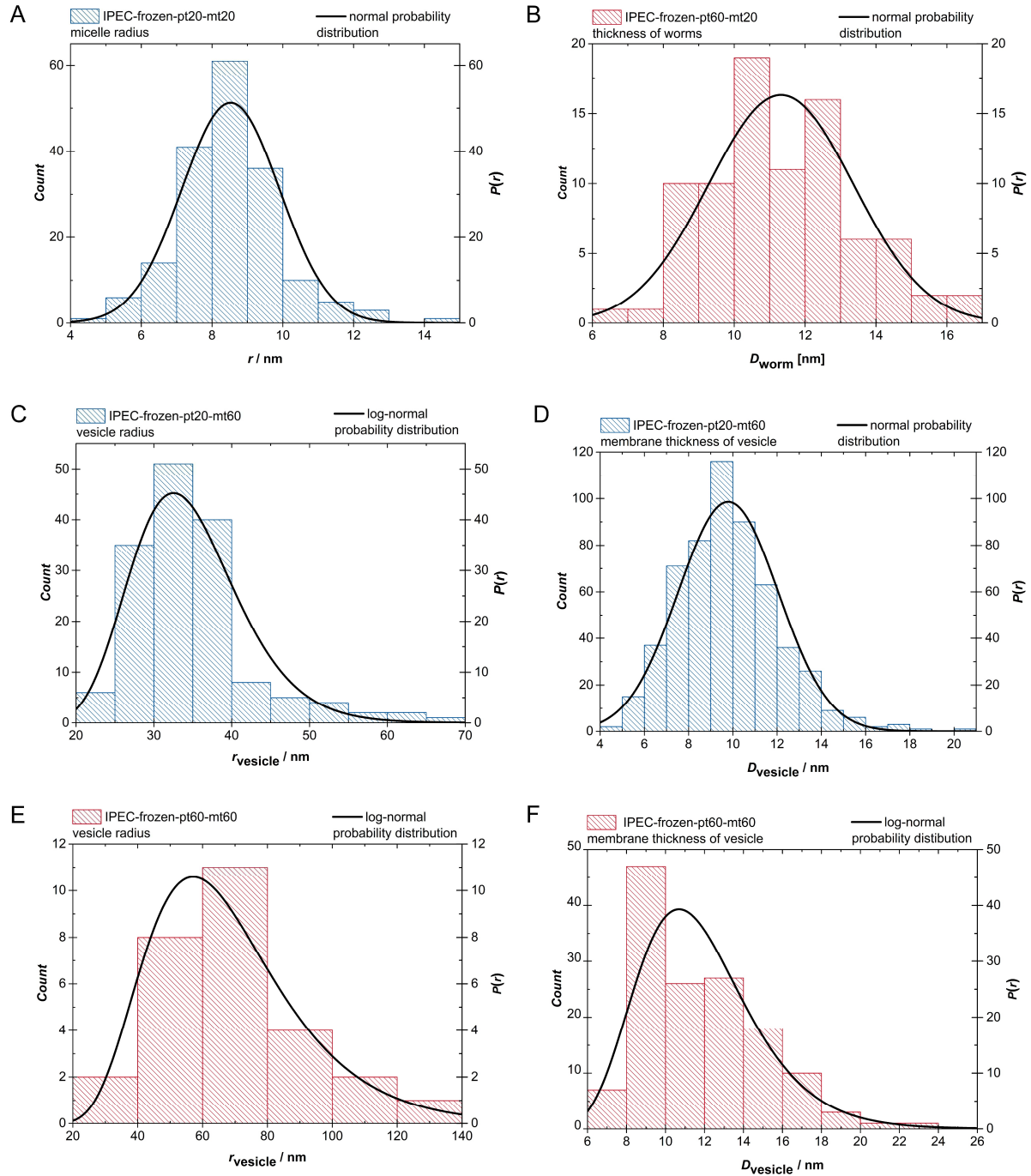


Figure S8. Histograms of size distributions obtained from cryo-TEM analysis: (A) distribution of the radius of 178 spherical-like objects measured for IPEC-frozen-pt20-mt20 (cf. Figure 3A); (B) distribution of the thickness of 12 worm-like objects (determined at 7 positions of each object) measured for IPEC-frozen-pt60-mt20 (cf. Figure 3D); (C) distribution of the radius (including the visible membrane) of 154 vesicular objects measured for IPEC-frozen-pt20-mt60 (cf. Figure 3B); (D) distribution of the visible membrane thickness of 56 vesicular objects (determined at 10 positions of each object) measured for IPEC-frozen-pt20-mt60 (cf. Figure 3B); (E) distribution of the radius (including the visible membrane) of 28 vesicular objects measured for IPEC-frozen-pt60-mt60 (cf. Figure 3C); (F) distribution of the visible membrane thickness of 28 vesicular objects (determined at 5 positions of each object) measured for IPEC-frozen-pt60-mt60 (cf. Figure 3C).

Structural Parameters of Kinetically Frozen IPEC Micelles

The following table summarizes the micellar sizes obtained from DLS, SANS and cryo-TEM analysis. The hydrodynamic radius R_h measured at 60 °C clearly indicates the difference between the IPEC samples kinetically frozen at 20 and 60 °C. These average R_h include vesicles and irregular aggregates in case of IPEC-frozen-pt20-mt60 and vesicles as well as worm-like assemblies for IPEC-frozen-pt60-mt60. The size of the vesicular objects was analyzed via cryo-TEM. The vesicle radius given in Table S5 includes those membrane parts visible in the cryo-TEM images. The thickness of these parts is presented as D_{vesicle} excluding the outer and inner parts of the membrane, which is supposed to be water-soluble PEO chains with an insufficient contrast.¹⁷⁻¹⁹ The sizes obtained for the samples vitrified at room temperature mainly describe the dimensions of the micellar IPEC cores, which is the only insoluble part at 20 °C and exhibits the best contrast for cryo-TEM analysis. In case of IPEC-frozen-pt20 a small spherical-like complex is formed, whereas for IPEC-frozen-pt60 the images show an elongated, worm-like core structure. As discussed above, also further evaluation of the DLS data indicate the formation of elongated objects. The sizes obtained from SANS data fitting applying a core-shell (cs) cylinder form factor fit correspond well with the cryo-TEM analysis. A spherical cs form factor was fitted to the scattering pattern of IPEC-frozen-pt20-mt20. For both fits equivalent overall radii were obtained. For the evaluation of the SANS measurements performed at 60 °C a sum of two form factors were applied based on the structural information received from cryo-TEM images. A hollow cs sphere simulates the vesicular structure, whereas fractal aggregates consisting of cs spheres depict the irregular aggregates observed for IPEC-frozen-pt20-mt60. Also for the sample IPEC-frozen-pt60-mt60 a simple cs sphere with a hollow core was used to describe the vesicular objects and a cylinder form factor was applied for the elongated assemblies (due to the considerable number of parameters in the fitting process, the inner core-shell structure of the worms was neglected here).

Table S5. Comparison of structural parameters (in nm) of kinetically frozen IPEC micelles prepared at different temperatures (20 °C and 60 °C), diluted and measured at different temperatures obtained from DLS, cryo-TEM and SANS data analysis.

sample ^[a]	R_h	cryo-TEM ^[b]	SANS data fitting ^{[b],[d]}
IPEC-frozen-pt20-mt20	17 ± 1	$R_c = 8.5 \pm 1.4$	cs-sphere: $R_c = 6.8 (0.32)$ $D_s = 4.7 (0.01)$
IPEC-frozen-pt60-mt20	18 ± 1	$D_c = 11.3 \pm 2.1$ $L_c = 90.5 \pm 22$	cs-cylinder: $R_c = 4.7 (0.33)$ $D_s = 5.9 (0.42)$ $L = 153.7 (0)$
IPEC-frozen-pt20-mt60	30 ± 1	$R_{\text{vesicle}} = 34.7 \pm 7.9^{[c]}$ $D_{\text{vesicle}} = 9.8 \pm 2.3$	hollow cs-sphere: $R_c = 8.6 (0.23)$ $D_s = 18.5 (0.12)$ fractal cs-sphere aggregates: $R_c = 13.8 (0.30)$ $D_s = 9.3 (0.03)$ $\zeta = 19.3$

IPEC-frozen- pt60-mt60	48 ± 1	$R_{\text{vesicle}} = 68.2 \pm 22.7^{[c]}$ $D_{\text{vesicle}} = 11.8 \pm 3.2$	cylinder:
			$R = 17.4 (0.50)$
			$L = 94.1 (0)$
			hollow cs-sphere:
			$R_c = 28.6 (0.78)$ $D_s = 17.5 (0.01)$

[a] pt: preparation temperature, mt: measurement temperature. [b] R : radius, D : thickness, L : length, ξ : correlation length, c: core, s: shell. [c] vesicle radius includes membrane parts visible in cryo-TEM. [d] number in () represents the polydispersity index.

2.2. Structure Freezing by Dialysis

Another way to drastically reduce the concentration of the low molecular weight salt is dialysis against salt-free water. The dialysis was conducted at the same temperatures as the samples previously were prepared and equilibrated. Thus, it was expected that the obtained equilibrium micellar morphology is not changed upon exchange of the salt solution for pure D₂O.

In contrast to the dilution approach, the polymer concentration does not considerably change during the procedure. Further, dialysis is as opposed to dilution a rather slow process which might enable rearrangements upon continuous reduction of the salt content. These differences might finally result in kinetically frozen structures that differ from the equilibrium morphologies as well as from those assemblies frozen by dilution.

After termination of the dialysis, the samples prepared at 60 °C and at room temperature visibly differed in their turbidity after storage at room temperature (Figure S9). As they were prepared from the same stock solutions, the dialyzed samples contain the same polymer concentration. Hence, the considerably increased turbidity of the sample prepared at $T > \text{LCST}$ might result from large aggregates or even from different micellar structures of higher order morphologies such as worms or vesicles.²⁰

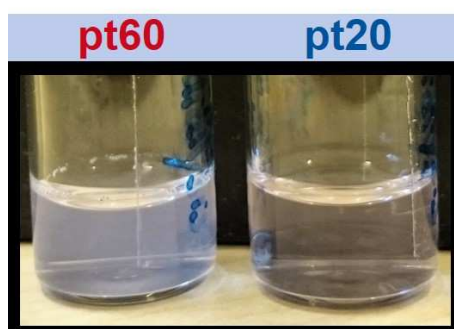


Figure S9. Pictures of IPEC samples, stored at room temperature for 20 h after termination of equilibration and subsequent dialysis at 20 °C (pt20) and 60 °C (pt60).

DLS Results

Micellar IPEC assemblies that were kinetically frozen by eliminating the low molecular weight salt via dialysis at different temperatures show the same general temperature-dependent trend for their

hydrodynamic radii (Figure S10A). Reaching the LCST of PNIPAM a substantial increase in size is observed. In comparison to the diluted IPEC assemblies, however, the samples dialyzed at different temperatures do not exhibit distinctly different hydrodynamic radii at temperatures above the LCST. The hydrodynamic size of the micelles is rather similar for both preparation temperatures over the whole temperature range. This might indicate that the same structures are formed irrespective of the preparation temperature. In contrast to the dilution pathway, CONTIN analysis reveals considerable standard deviations of the average R_h for $T > \text{LCST}$. This is also clear from the Γ vs. q^2 plot, which especially suggests the presence of polydisperse assemblies at 60 °C (Figure S10B). Therefore, it is important to consider that here the y-intercept cannot be regarded necessarily as a hint for structural anisotropy. The DLS data measured at 20 °C, however, yield R_h with much smaller deviations. Here Γ vs. q^2 exhibits a y-intercept of zero for IPEC-dialyzed-pt20 and an intercept distinctly different from zero for IPEC-dialyzed-pt60. As explained above this is not expected for polymeric micelles and hence the following interpretation should be treated with caution. The y-intercept might indicate that elongated IPEC structures are present at 20 °C when the preparation is performed at temperatures above the LCST of PNIPAM, whereas a preparation at $T < \text{LCST}$ does not induce the formation of particles with additional relaxation processes. Similar to the sample kinetically frozen by dilution, the expression for the diffusion of rigid rods established by Tirado and Garcia de la Torre (see above) can be applied to calculate rod length and diameter for the elongated species of IPEC-dialyzed-pt60 at 20 °C exhibiting an equivalent sphere R_h of 16 nm with $D_T = 1.088 \cdot 10^{-11} \text{ m}^2\text{s}^{-1}$. For given diameters of 11, 15 and 20 nm rod lengths of 73, 58 and 41 nm are obtained. As stated above these calculations depict good approximations and the hypothesis of the presence of worm-like objects can be further verified with the help of SANS measurements.

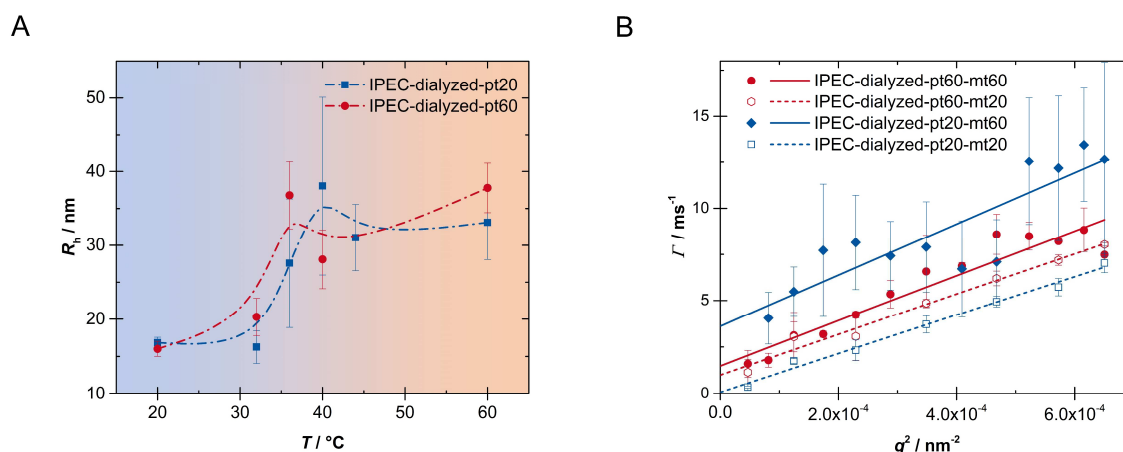


Figure S10. (A) Temperature dependence of the average R_h of IPEC micelles kinetically frozen by dialysis of an equilibrated solution measured by DLS for different preparation temperatures (pt). The polymer concentration is about 0.62 wt%. The dashed lines are guides to the eyes. (B) Average decay rate Γ obtained by CONTIN analysis of DLS results of IPEC micelles frozen by dialysis plotted versus q^2 .

SANS Results

Comparing the SANS patterns obtained at 20 °C for different preparation temperatures reveals different slopes in the low q -region as indicated by the dashed lines (Figure S11A). The first data points are neglected as they probably result from the scattering of a few loose aggregates. A q^{-1} dependence is

typically found for rod-like assemblies. With that the scattering data measured for IPEC-dialyzed-pt60-mt20 gives rise to the assumption that worm-like assemblies have formed, which is supported by the DLS results as described above. IPEC-dialyzed-pt20-mt20 in comparison exhibits a much flatter decreasing scattering intensity for small q values. This qualitative treatment of the SANS data suggests the formation of differently shaped micellar assemblies at temperatures below the LCST of PNIPAM for different preparation temperatures and hence proposes a successful freezing of equilibrium structures via the dialysis approach.

To describe the entirely measured q range, form factor fits consisting of three individual models were applied. For both preparation temperatures, the low- q region was fitted with a simple sphere to model large loose aggregates, which were also found in DLS analysis, and the high- q region was described with a Lorentzian function. For the sample prepared at 20 °C the mid- q region is well described by a spherical core-shell form factor (Figure S11A: blue squares and grey line). As Table S6 shows the obtained sizes are very similar to those obtained for IPEC-frozen-pt20-mt20, which was kinetically trapped by dilution (compare Table S4). The core structure of this model describes the IPEC domain, whereas the shell depicts the hydrated corona containing long PEO arms as well as short PNIPAM blocks as illustrated in Scheme S2E. The mid- q region measured for IPEC-dialyzed-pt60-mt20 is described by a cylindrical core-shell form factor (Figure S11A: red circles and black line). The same location for the polymeric domains is assumed here with the IPEC in the core and PEO as well as PNIPAM within the shell (compare Scheme S2F). The length of the cylindrical micelle obtained from fitting is especially error-prone as the q^{-1} region is partly superimposed by the scattering resulting from loose aggregates.

At $T > \text{LCST}$ the scattering patterns look rather similar at first glance, both exhibiting four regions with different q dependencies (Figure S11B). For the low- and intermediate- q regime, however, the scattering behavior is slightly different for both preparation temperatures. Both curves show a small bump in the measured scattering intensity for the region with a q dependence of about q^{-3} , which is not characteristic for any particular morphology. For q values approaching 0.001 \AA^{-1} the scattering pattern of IPEC-dialyzed-pt60-mt60 exhibits a slope of approximately q^{-1} , which might indicate the presence of elongated assemblies. In contrast, for the sample dialyzed at room temperature and measured at 60 °C the scattering data suggest a spherical-like micellar assembly.

For further analysis of the scattering data by form factor fitting the same models that were applied for IPEC-frozen-mt60 were used. The sample IPEC-dialyzed prepared at 20 °C and measured at 60 °C is nicely described by the combination of a hollow sphere and a fractal aggregate from core-shell spheres (Figure S11B: blue squares and grey line, compare Scheme S2E). The shell of the hollow sphere model contains all micellar domains (IPEC, dehydrated PNIPAM, PEO corona). Apart from the vesicles also the fractal aggregates result from the aggregation of the spherical cs micelles present at 20 °C due to dehydration of PNIPAM. The core of these aggregated spheres now contains the IPEC domain as well as the dehydrated PNIPAM, whereas the shell is only occupied by PEO. A comparison of Table S6 and Table S4 again shows that very similar results are obtained for IPEC-frozen-pt20-mt60 and IPEC-dialyzed-pt20-mt60. The scattering data measured for IPEC-dialyzed-pt60-mt60 are rather well described by a combination of a hollow sphere and a cylindrical micelle (Figure S11B: red circles and black line, compare Scheme S2F). In comparison to IPEC-frozen-pt60-mt60 the thickness of the vesicle and the radius of the cylindrical assembly are the same. This might indicate that the objects frozen by dialysis exhibit the same inner structure as those frozen by dilution. Only the overall size, which is estimated from the inner vesicle radius and the length of the cylinder, differs for both preparation pathways.

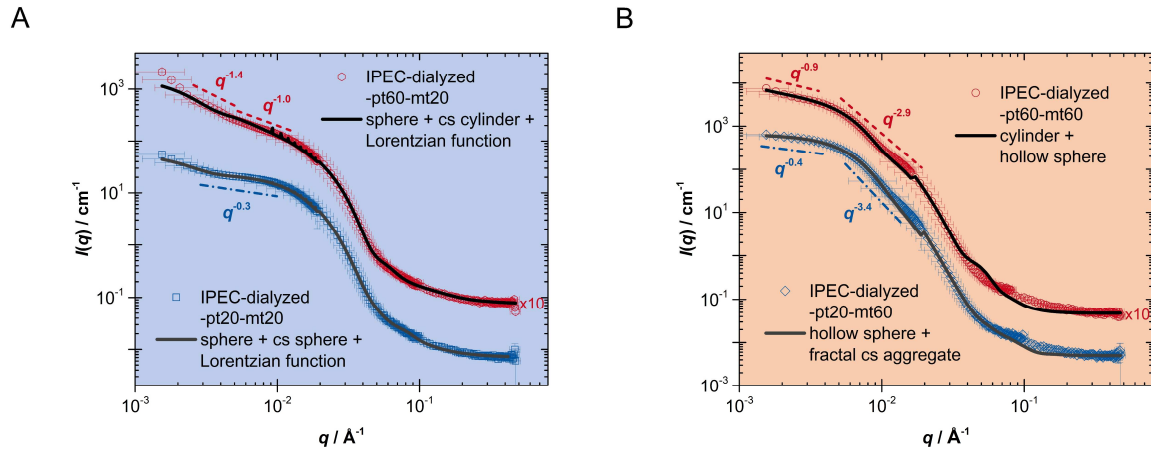
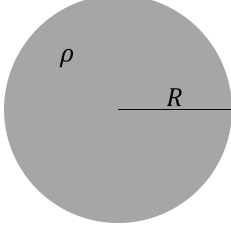
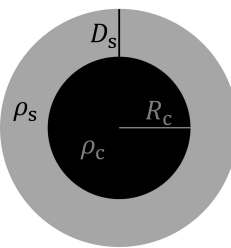
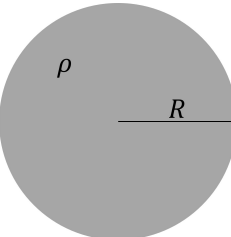
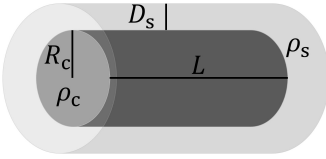
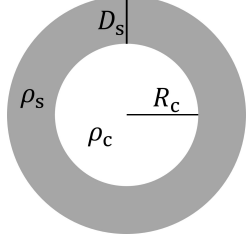
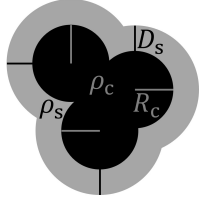
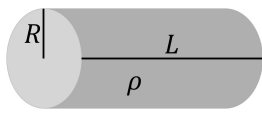
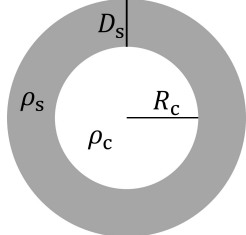


Figure S11. Scattering curves of IPEC micelles kinetically frozen by dialysis of an equilibrated solution measured (mt) at 20 °C (A) and 60 °C (B) for different preparation temperatures (pt). The polymer concentration is about 0.62 wt%. The solid lines represent form factor fits as indicated in the legend. For clarity, the intensity data for samples prepared at 60 °C are shifted vertically (x10).

Table S6. Structural parameters of kinetically frozen IPEC micelles prepared at different temperatures (20 °C and 60 °C), dialyzed and measured at different temperatures obtained from SANS data analysis. The corresponding SANS data and form factor fits are presented in Figure S11.

sample	form factor model	fit results
		spherical aggregate: $R = 111.0 \text{ nm}$ (σ set to 0) $\rho = 4.5 \cdot 10^{-6} \text{ \AA}^{-1}$
IPEC-dialyzed -pt20-mt20		spherical core-shell micelle: $R_c = 7.2 \text{ nm}$ ($\sigma_c = 0.11$) $D_s = 5.6 \text{ nm}$ ($\sigma_s = 0.58$) $\rho_c = 3.7 \cdot 10^{-6} \text{ \AA}^{-1}$ $\rho_s = 5.5 \cdot 10^{-6} \text{ \AA}^{-1}$
		Lorentzian function: $\xi = 10.2 \text{ nm}$
IPEC-dialyzed -pt60-mt20		spherical aggregate: $R = 117.2 \text{ nm}$ (σ set to 0) $\rho = 5.9 \cdot 10^{-6} \text{ \AA}^{-1}$

		cylindrical core-shell micelle: $R_c = 5.6 \text{ nm}$ ($\sigma_c = 0.19$) $D_s = 3.8 \text{ nm}$ ($\sigma_s = 0.01$) $L = 103.3 \text{ nm}$ (σ set to 0) $\rho_c = 4.4 \cdot 10^{-6} \text{ \AA}^{-1}$ $\rho_s = 5.3 \cdot 10^{-6} \text{ \AA}^{-1}$
		Lorentzian function: $\zeta = 8.0 \text{ nm}$
IPEC-dialyzed -pt20-mt60		hollow sphere (vesicle): $R_c = 10.9 \text{ nm}$ ($\sigma_c = 0.01$) $D_s = 18.9 \text{ nm}$ ($\sigma_s = 0.46$) $\rho_c = 6.4 \cdot 10^{-6} \text{ \AA}^{-1}$ (fixed) $\rho_s = 4.9 \cdot 10^{-6} \text{ \AA}^{-1}$
		fractal aggregate from core-shell spheres: $R_c = 12.3 \text{ nm}$ ($\sigma_c = 0.61$) $D_s = 7.1 \text{ nm}$ ($\sigma_s = 0.01$) $\rho_c = 3.4 \cdot 10^{-6} \text{ \AA}^{-1}$ $\rho_s = 5.3 \cdot 10^{-6} \text{ \AA}^{-1}$ $D_f = 2.6$ $\zeta = 11.1 \text{ nm}$
IPEC-dialyzed -pt60-mt60		cylindrical micelle: $R = 17.5 \text{ nm}$ ($\sigma = 0.22$) $L = 1350 \text{ nm}$ (σ set to 0) $\rho = 4.8 \cdot 10^{-6} \text{ \AA}^{-1}$
		hollow sphere (vesicle): $R_c = 13.0 \text{ nm}$ ($\sigma_c = 0.61$) $D_s = 18.5 \text{ nm}$ ($\sigma_s = 0.11$) $\rho_c = 6.4 \cdot 10^{-6} \text{ \AA}^{-1}$ (fixed) $\rho_s = 4.4 \cdot 10^{-6} \text{ \AA}^{-1}$

pt: preparation temperature, mt: measurement temperature, R : radius, D : thickness, L : length, ζ : correlation length, ρ : scattering length density, σ : polydispersity, c: core, s: shell, D_f : fractal dimension.

IFTs of the scattering data measured at 20 °C for $q > 0.0045 \text{ \AA}^{-1}$ support the conclusions drawn from the qualitative consideration of the scattering curves (Figure S12A). The PDDF of IPEC-dialyzed-pt20-mt20 suggests the presence of spherical-like micellar assemblies, whereas the long-drawn-out decrease for large distances r of IPEC-dialyzed-pt60-mt20 indicates the formation / preservation of worm-like micelles.

The PDDF of the IPEC micelles generated at 60 °C after equilibration and dialysis at room temperature shows a clear spherical structure (Figure S12B). For IPEC-dialyzed-pt60-mt60 the PDDF is slightly

flattened for distances r of 200-400 Å. This might be an indication for the formation of vesicular structures, whereas the PDDF does not suggest the presence of elongated worm-like structures. As we probably obtain at least two coexisting micellar species at temperatures above the LCST of PNIPAM it is however not possible to draw distinct conclusions on the assembly shape from the PDDFs.

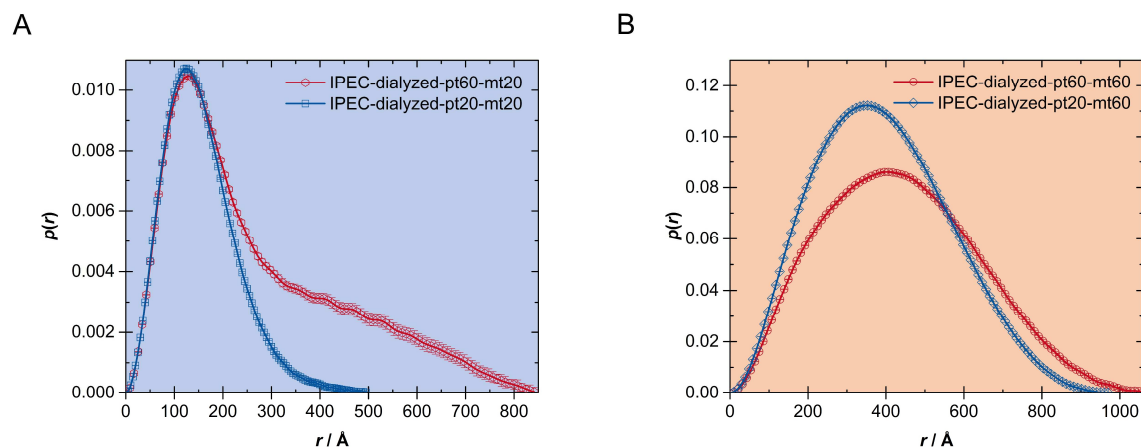


Figure S12. PDDFs calculated via IFT from the scattering data of IPEC-dialyzed measured at 20 °C (A) and 60 °C (B).

2.3. Interpolyelectrolyte Complexation without Salt

DLS Results

For comparison, the complexation between STAR and DIBLOCK is finally performed without addition of any low molecular weight salt. It is expected that more ill-defined aggregates will develop on behalf of equilibrium micellar assemblies as dynamic exchange reactions will not occur in the absence of salt. Therefore, a considerable difference in morphology is not expected for different preparation temperatures, taking also into account the substantially increased unimer concentration for the pure DIBLOCK solution even in the heat (electrostatic repulsion in the highly charged corona lowers aggregation number and increases critical micelle concentration/temperature of the thermosensitive DIBLOCK). As Figure S13A shows, both samples, differing in their preparation temperature, exhibit the same temperature-dependent change of R_h and under consideration of the error bars approximately the same sizes. Again, highly polydisperse micellar assemblies are observed at temperatures above the LCST of PNIPAM whereas substantially more uniform particles are formed below the LCST. The Γ vs. q^2 plot might reveal the formation of anisotropic structures for IPEC-no-salt-pt20 at 20 °C as the y-intercept is unlike zero (Figure S13B). The increase in size upon heating to temperatures above the LCST results from the aggregation of partly dehydrated PNIPAM blocks. As rearrangements of the IPEC domains are prevented due to the lack of low molecular weight salts, the formation of polydisperse structures might be favored.

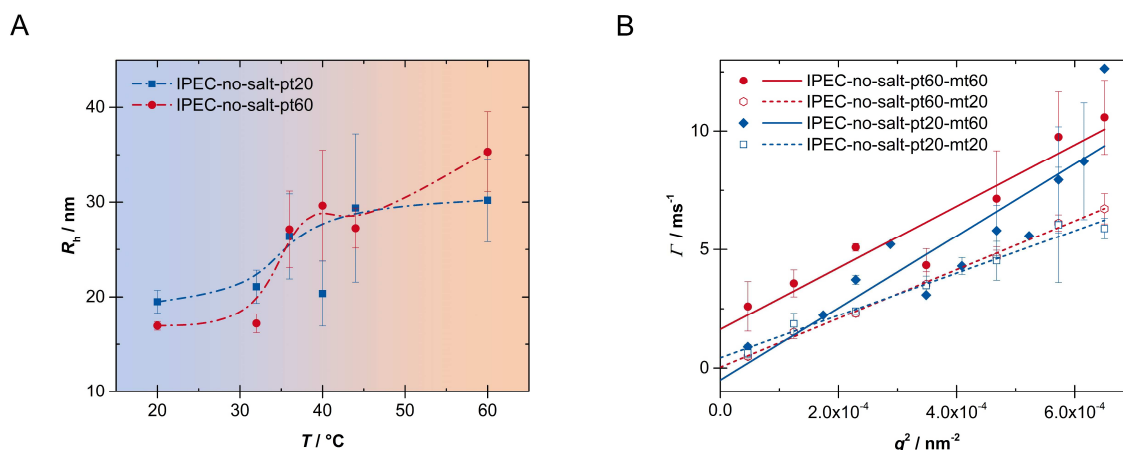


Figure S13. (A) Temperature dependence of the average R_h of IPEC micelles in D₂O measured by DLS for different preparation temperatures (pt). The polymer concentration is about 0.65 wt%. The dashed lines are guides to the eyes. (B) Average decay rate Γ obtained by CONTIN analysis of DLS results of IPEC micelles in D₂O plotted versus q^2 .

SANS Results

The SANS data measured at 20 °C for the IPEC samples prepared in absence of salt are the same for both preparation temperatures except for a slight difference in the q -dependence at small scattering vectors (Figure S14A). However, the scattering patterns might be regarded as almost the same, in both cases suggesting the formation of possibly slightly elongated micelles. Form factor fitting yielded best results for an ellipsoidal core-shell model in the mid- q region of the scattering curve (Figure S14A, compare Scheme S2C,D). The results presented in Table S7 show that the ellipsoidal assembly prepared at 60 °C is slightly larger (5 nm / 3 nm in equatorial / polar diameter) compared to that prepared at 20 °C. Under the assumption of similar densities of the IPEC domain, this might suggest a bigger aggregation number for IPEC-no-salt-pt60-mt20. Hence, this indicates that the temperature influences the IPEC formation. Nevertheless, the micellization process is dominated by the rapid IPEC formation rather than the dehydration and aggregation of PNIPAM at 60 °C. Consequently, the same structures are obtained at 20 °C irrespective of the preparation temperature. For the description of the low- and high- q region, the scattering data were again rather well described by a Lorentzian function and a monodisperse sphere, respectively.

The scattering curves obtained at 60 °C both exhibit a q^{-2} decrease at low q -values, which is typical for flat particles or vesicular structures (Figure S14B). Further, both patterns show a slight bump in the low q -regime, which is more pronounced and found at slightly higher q for the sample prepared at 20 °C. From these qualitative considerations, it might be deduced that vesicles of slightly different sizes have formed at $T > \text{LCST}$ for different preparation temperatures for an IPEC preparation without any salt added. A simple hollow sphere model was, however, not sufficient to describe the scattering curves of IPEC-no-salt-mt60. The combination of a hollow sphere and a spherical assembly yields much better results as depicted in Figure S14B and Table S7 (compare Scheme S2C, D). Also, the PDDFs suggest the formation of two or more coexisting species (Figure S15B). The fit results show that bigger vesicles are formed for a preparation at 60 °C. This is in line with the bigger ellipsoidal structures obtained at 20 °C after preparation at 60 °C. The spherical objects that might have formed in addition are, however, of similar sizes for both preparation temperatures. This species might be irregular aggregates similar to those found for IPEC-frozen-pt20-mt60.

In comparison with all previously discussed scattering curves, those from IPEC-no-salt show a steeper decay of $q^{-1.5}$ to $q^{-2.0}$ at high q values indicating a denser internal structure. This might result from the prevented rearrangement processes involved in equilibration. However, modelling this region, e.g., with a Lorentzian function, in combination with the other models used (hollow sphere and sphere) was not successful for the measurement at 60 °C.

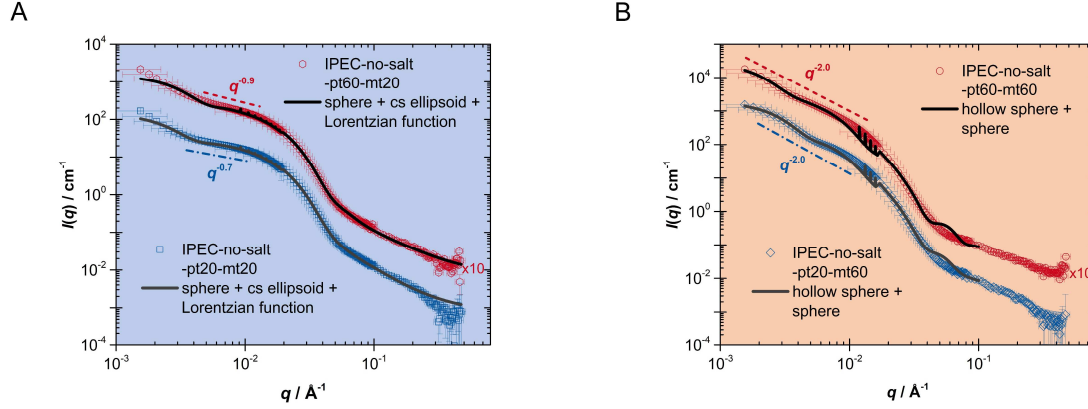
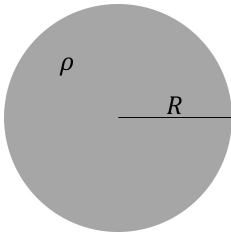
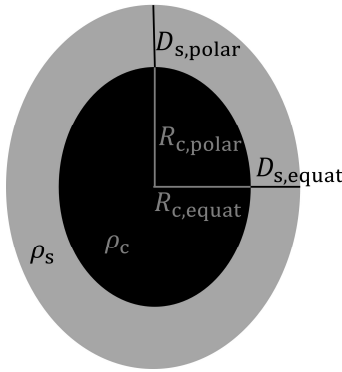
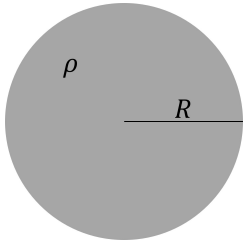
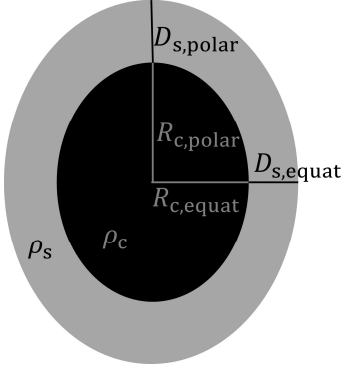
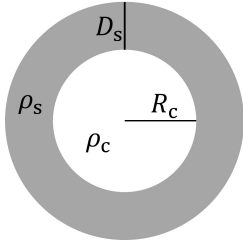
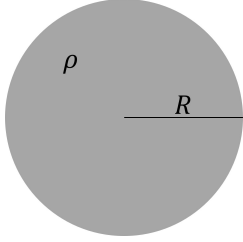
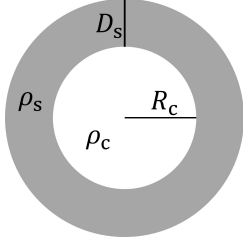
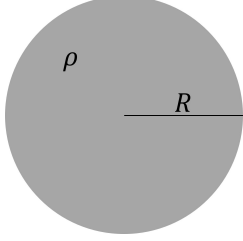


Figure S14. Scattering curves of IPEC micelles in D₂O measured (mt) at 20 °C (A) and 60 °C (B) for different preparation temperatures (pt). The polymer concentration is about 0.65 wt%. For clarity, the intensity data for samples prepared at 60 °C are shifted vertically (x10).

Table S7. Structural parameters of kinetically frozen IPEC micelles prepared in D₂O at different temperatures (20 °C and 60 °C) and measured at different temperatures obtained from SANS data analysis.

sample	form factor model	fit results
		spherical aggregate: $R = 101.3 \text{ nm}$ (σ set to 0) $\rho = 4.4 \cdot 10^{-6} \text{ \AA}^{-1}$
IPEC-no-salt -pt20-mt20		ellipsoidal core-shell micelle: $R_{c,eqat} = 6.4 \text{ nm}$ ($\sigma_c = 0.36$) $x_c = 1.34$ (σ set to 0) $\rightarrow R_{c,polar} = 8.6 \text{ nm}$ $D_{s,eqat} = 3.3 \text{ nm}$ ($\sigma_s = 0.39$) $x_s = 4.39$ (σ set to 0) $\rightarrow D_{s,polar} = 14.5 \text{ nm}$ $\rho_c = 3.5 \cdot 10^{-6} \text{ \AA}^{-1}$ $\rho_s = 5.5 \cdot 10^{-6} \text{ \AA}^{-1}$
		Lorentzian function: $\zeta = 2.4 \text{ nm}$

		spherical aggregate: $R = 81.3 \text{ nm}$ (σ set to 0) $\rho = 4.7 \cdot 10^{-6} \text{ \AA}^{-1}$
IPEC-no-salt -pt60-mt20		ellipsoidal core-shell micelle: $R_{c,equat} = 7.9 \text{ nm}$ ($\sigma_c = 0.22$) $x_c = 1.73$ (σ set to 0) $\rightarrow R_{c,polar} = 13.7 \text{ nm}$ $D_{s,equat} = 3.3 \text{ nm}$ ($\sigma_s = 0.78$) $x_s = 3.60$ (σ set to 0) $\rightarrow D_{s,polar} = 11.9 \text{ nm}$ $\rho_c = 3.6 \cdot 10^{-6} \text{ \AA}^{-1}$ $\rho_s = 6.0 \cdot 10^{-6} \text{ \AA}^{-1}$
		Lorentzian function: $\zeta = 1.0 \text{ nm}$
IPEC-no-salt -pt20-mt60		hollow sphere (vesicle): $R_c = 40.9 \text{ nm}$ ($\sigma_c = 0.44$) $D_s = 17.1 \text{ nm}$ ($\sigma_s = 0.13$) $\rho_c = 6.4 \cdot 10^{-6} \text{ \AA}^{-1}$ (fixed) $\rho_s = 4.5 \cdot 10^{-6} \text{ \AA}^{-1}$
		sphere: $R = 29.0 \text{ nm}$ ($\sigma = 0.01$) $\rho = 4.6 \cdot 10^{-6} \text{ \AA}^{-1}$
IPEC-no-salt -pt60-mt60		hollow sphere (vesicle): $R_c = 54.7 \text{ nm}$ ($\sigma_c = 0.57$) $D_s = 16.2 \text{ nm}$ ($\sigma_s = 0.07$) $\rho_c = 6.4 \cdot 10^{-6} \text{ \AA}^{-1}$ (fixed) $\rho_s = 4.0 \cdot 10^{-6} \text{ \AA}^{-1}$
		sphere: $R = 31.5 \text{ nm}$ ($\sigma = 0.01$) $\rho = 4.7 \cdot 10^{-6} \text{ \AA}^{-1}$

pt: preparation temperature, mt: measurement temperature, R : radius, D : thickness, L : length, ξ : correlation length, ρ : scattering length density, σ : polydispersity, x : ratio of polar to equatorial dimension, c: core, s: shell, equat: equatorial.

The PDDFs calculated for the IPEC assemblies prepared without any salt added at room temperature indicate that slightly elongated assemblies formed upon complexation (Figure S15A).

For a measurement temperature of 60 °C the PDDF of IPEC-no-salt-pt20 implies the presence of vesicular structures due to the flat shoulder for approximately 300-700 Å (Figure S15B). This also applies to the sample prepared at $T > \text{LCST}$. In this case, however, the PDDF course gives the impression that vesicles of different sizes are formed.

These results confirm that at least very similar micellar structures are formed at 20 and 60 °C upon interpolyelectrolyte complexation without any low molecular weight salt added into the system.

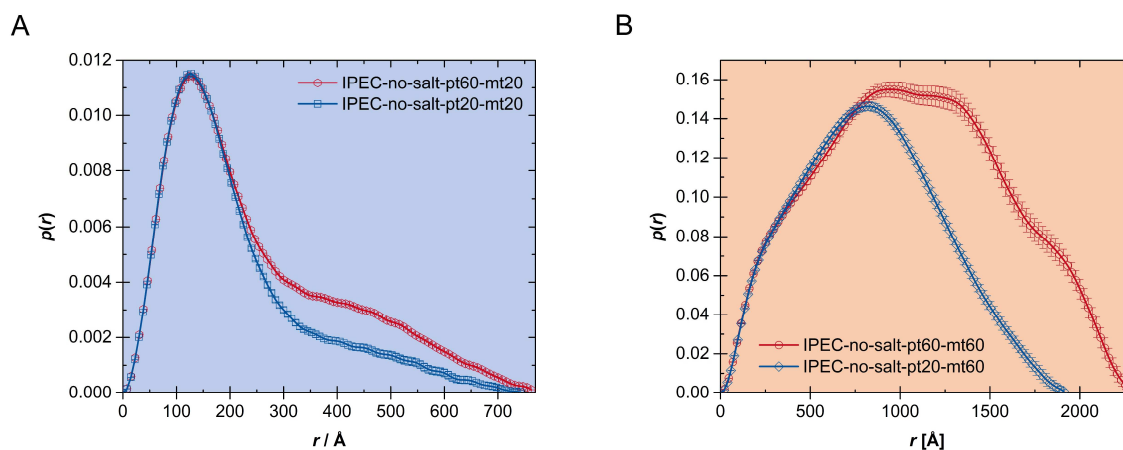


Figure S15. PDDFs calculated via IFT from the scattering data of IPEC-no-salt measured at 20 °C (A) and 60 °C (B).

2.4. Concentrated Equilibrated IPEC Solution

Concentrated polymer solutions served as equilibrated stock solutions for the dilution approach. These were also investigated by means of SANS. Unfortunately, the neutron beam could not be aligned appropriately as the available volume of the solution was insufficient to fill the cuvettes. Thus, scattering effects caused by the interface are responsible for the steeply increasing scattering intensity at low q -values (Figure S16). Apart from this the scattering patterns detected at 20 °C and 60 °C seem to be almost identical for both preparation temperatures as it was expected from a previous study of the equilibrated IPECs.¹

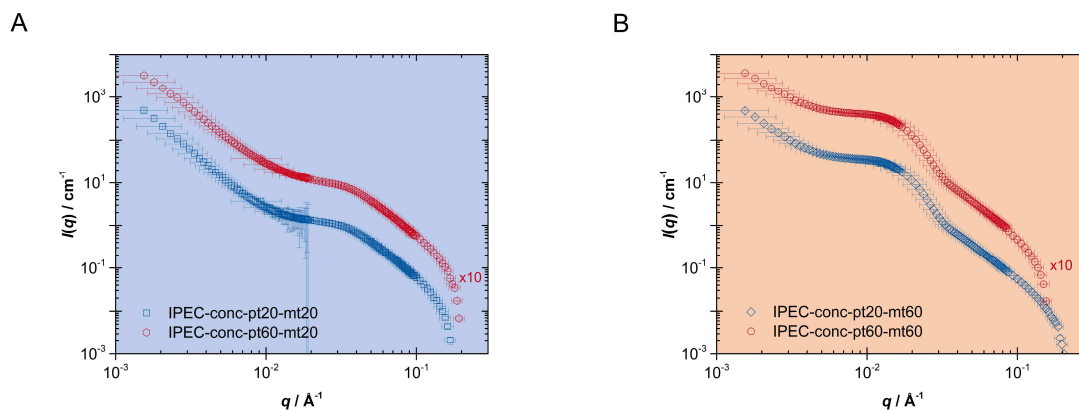


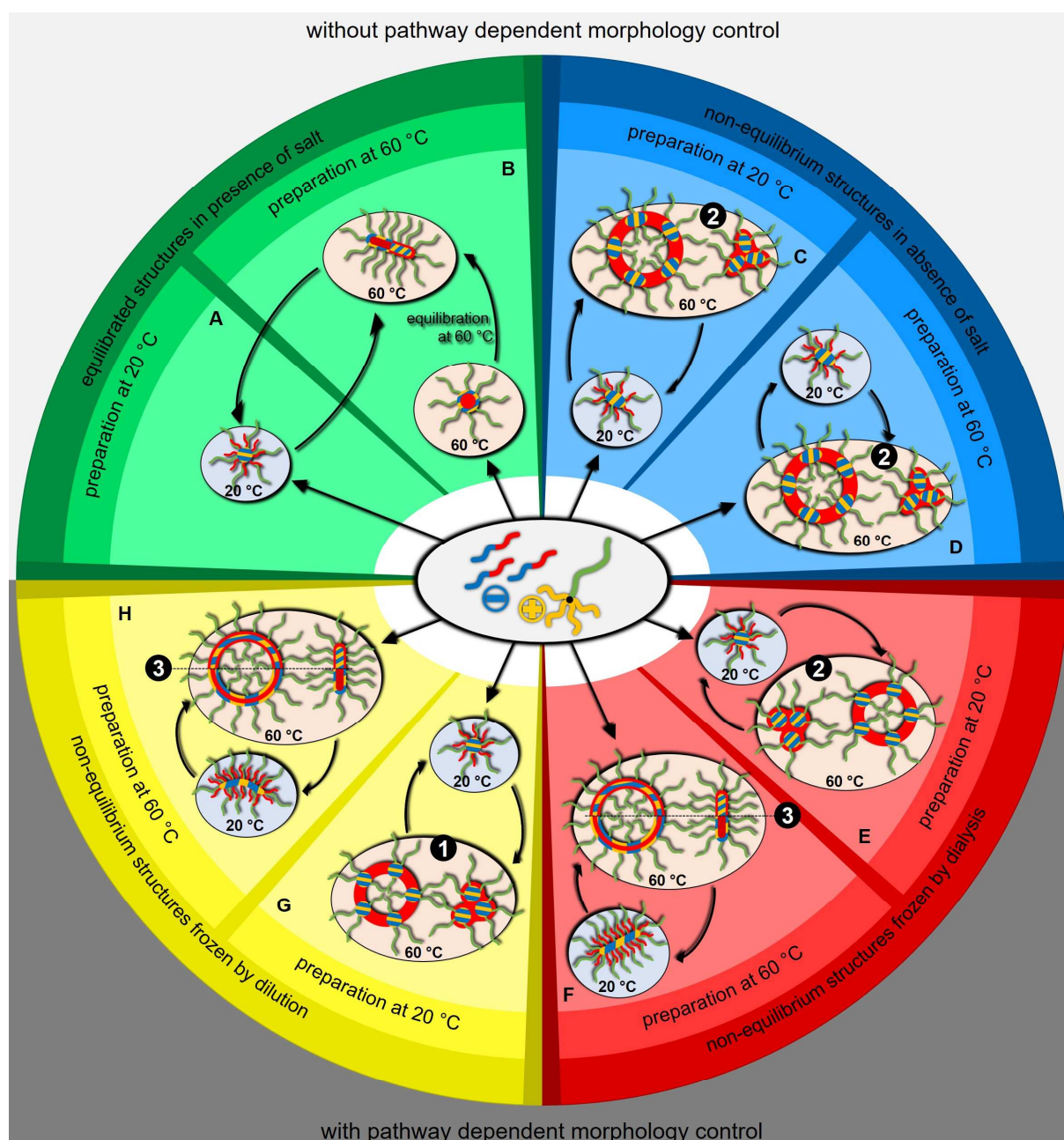
Figure S16. Scattering curves of IPEC micelles in 0.3 M NaCl (D_2O) measured (mt) at 20 °C (A) and 60 °C (B) for different preparation temperatures (pt). The polymer concentration is about 9.8 wt%. For clarity, the intensity data for samples prepared at 60 °C are shifted vertically (x10).

2.5. Comparative Discussion

In order to stabilize various nonequilibrium micellar IPEC structures, a temperature-responsive polyelectrolyte system was applied exhibiting different quasi-equilibrium morphologies below and above the LCST of PNIPAM (green quarter in Scheme S2). Spherical core-corona assemblies were found at $T < \text{LCST}$ with a water-insoluble IPEC core and a two-component corona consisting of short PNIPAM blocks and long PEO arms (Scheme S2A).¹ Equilibration at $T > \text{LCST}$ results in the formation of worm-like micellar morphologies probably of core-shell-corona structure (Scheme S2B).¹ The water-soluble corona is composed of the PEO arms, whereas the IPEC domain forms the core surrounded by a PNIPAM shell or vice versa as discussed in Ref. 2.

In case of polyelectrolyte systems, equilibrium interpolyelectrolyte complex micellar assemblies are always obtained in the presence of a low molecular weight salt. Within certain system-dependent limits, this enables a dynamically progressive exchange of single polyions between different (micellar) co-assemblies.^{21,22} Exchange reactions are suppressed if the salt concentration is below the lower limit, whereas no IPEC micelles are found as the charges of the polyions are completely screened by the low molecular weight ions preventing complex formation at salt contents above the upper limit. Thus, to stabilize the different equilibrium micellar assemblies it is necessary to remove the salt or at least drastically reduce the salt concentration to inhibit rearrangements. Two possible pathways were tested to kinetically freeze IPEC micelles at different temperatures allowing access to a directed creation of various morphologies from IPEC systems. In the first approach, a concentrated equilibrated IPEC solution was rapidly and drastically diluted. In a second approach, an IPEC solution was dialyzed against salt-free water after equilibration in presence of NaCl.

As a reference system, the IPEC formation was further performed without addition of any salt at temperatures below and above the LCST of PNIPAM directly resulting in kinetically frozen structures (blue quarter in Scheme S2). As the scattering studies of the salt-free samples discussed above reveal, there is almost no difference in the morphologies for the different preparation temperatures. Slightly elongated, possibly ellipsoidal, assemblies are present at 20 °C, which seem to exhibit a rather narrow size distribution. Polydisperse assemblies appear upon exceeding the temperature above the LCST of PNIPAM, which probably are of vesicular and spherical-like structure. Mixing STAR and DIBLOCK



- ① based on cryo-TEM
- ② in analogy to the structures found for IPEC-frozen-pt20-mt60 (G, 60 °C)
- ③ most probable core structure: above the dashed line (IPEC domain surrounded by dehydrated PNIPAM)²

Scheme S2. Representation of possible structures of IPECs at 20 °C and 60 °C for various preparation pathways.

dissolved in D₂O at room temperature results in the formation of ellipsoidally-shaped micellar assemblies with a kinetically frozen water-insoluble IPEC core surrounded by a two-component corona of water-soluble PEO and PNIPAM (Scheme S2C). If the temperature is increased above the LCST of PNIPAM these polymer blocks become dehydrated and consequently aggregate. This might result in vesicular structures and fractal aggregates of overall spherical shape as those depicted in Scheme S2C, as the IPEC domain is unable to undergo rearrangements. Upon heating the DIBLOCK solution to $T > \text{LCST}$ the formation of spherical micelles with a water-insoluble core containing the dehydrated PNIPAM blocks surrounded by a negatively charged corona of PVS blocks is expected.^{4,1} This is supposed to be especially favored in the presence of a low-molecular weight salt as an increase in the ionic strength leads to a reduced repulsion between the PVS blocks facilitating micelle formation and consequently reducing the critical micelle concentration (cmc). Hence, in absence of salt the cmc is supposed to be higher. Therefore, it is possible that here the DIBLOCK does not form spherical micelles at $T > \text{LCST}$. Upon addition of the STAR solution it is supposed that vesicles might be formed apart from fractal aggregates of spherical shape. When cooling to $T < \text{LCST}$ the PNIPAM blocks become water-soluble resulting in a disintegration of the obtained assemblies. The IPEC domain is unable to rearrange and ellipsoidal or elongated structures, possibly exhibiting a compartmentalized corona, might arise as depicted in Scheme S2D. As expected the obtained results indicate no considerable difference in the micellar shapes obtained for the complexation at different temperatures in absence of salt.

The first pathway to specifically generate nonequilibrium structures from IPECs is the dilution approach (yellow quarter in Scheme S2). The most important results of this are presented in the main part. It was clearly shown that it is possible to kinetically freeze various equilibrated IPEC assemblies by drastically and rapidly diluting a concentrated solution of these. Upon dilution at room temperature the spherical equilibrium core-corona structures are preserved (Scheme S2G). An increase in temperature leads to an aggregation of dehydrated PNIPAM blocks as soon as the LCST is exceeded. This results in the formation of irregular spherical-like and elongated aggregates as well as of vesicular structures (Scheme S2G), which probably exhibit a similar internal structure as described for the IPECs prepared without any salt. The water-insoluble spherical-like IPEC domains are distributed within a layer of collapsed PNIPAM blocks, which crosslink several smaller spherical micelles by aggregation. The water-soluble PEO arms are located at the inside as well as at the outside of this vesicular structure.¹⁷⁻¹⁹ The equilibration of an IPEC solution at $T > \text{LCST}$ results in the formation of mainly worm-like, partly branched, assemblies, which were also observed after dilution with salt-free water (Scheme S2H). After a decrease in temperature below the LCST of PNIPAM still and solely worm-like morphologies are present as shown by scattering and cryo-TEM investigations verifying that the dilution approach is a facile and successful pathway toward kinetically frozen nonequilibrium micellar IPECs. In cryo-TEM images these worms show almost entirely a bent shape (Figure 3D), which might either indicate a Janus-like composition of the micellar corona (with the short PNIPAM blocks at the stronger bent side and the longer PEO arms at the less bent side or vice versa when considering that at $Z = 1$ the number of PNIPAM blocks per micelle is two to three times higher compared to the number of PEO arms) or the curvature was preserved upon release from the curved surface of the vesicles. This former scenario might suggest that the PNIPAM blocks are located within the core of the vesicular- or worm-like assemblies at $T > \text{LCST}$, surrounded by an IPEC layer. Upon cooling, the dissolution of PNIPAM blocks results in a breakup of the worms, which curve due to the difference in required space of PNIPAM blocks on the one and PEO arms on the other side. However, this explanation does not regard merging of the IPEC domain and the reversible thermo-adjustment of size. Taking also previous discussion,² the opposite internal structure is probably more likely, exhibiting an IPEC domain in the interior of worms, shielded also by a PNIPAM shell, which keeps the IPEC domains apart even in the vesicles. Apart from

the worm-like micelles at 60 °C some vesicles were observed in cryo-TEM images. These seem to exhibit a rather uniform membrane, which is probably built up by association of the bent worm-like micelles.

The second approach toward a controlled creation of frozen nonequilibrium micellar IPEC assemblies is the dialysis pathway (red quarter in Scheme S2). As opposed to the dilution approach, DLS results did not show a clear difference between the samples prepared at room temperature and at $T > \text{LCST}$. SANS experiments, however, indicate that dialysis is likewise a successful method to freeze equilibrium IPEC structures and end up with different morphologies under the same final conditions depending on the preparation pathway. For a preparation temperature below the LCST of PNIPAM, a spherical-like core-corona micellar assembly is obtained just as for the diluted sample (Scheme S2E). Increasing the temperature to $T > \text{LCST}$ might similarly result in the formation of vesicular structures or spherical-like fractal aggregates as demonstrated in Scheme S2E. For a more precise statement, cryo-TEM images would be necessary. For the preparation at 60 °C, the obtained results reveal much clearer the formation of vesicular micelles (Scheme S2F). These might occur concomitant with elongated structures. The polydispersity is high as indicated by DLS results similarly to that of the IPEC prepared at room temperature and measured at 60 °C. Thus, further analysis is mandatory for distinct conclusions on the exact structure(s). The scattering results measured after decreasing the temperature to a value below the LCST, however, strongly suggest that worm-like micelles have formed. Hence, dialysis is also proven to be an appropriate and facile way to generate nonequilibrium micellar IPECs. The considerably different hydrodynamic radii observed for the dialyzed and diluted sample at $T > \text{LCST}$ for a preparation temperature of 60 °C might be accounted for by concentration effects. Before dilution, the IPEC solution exhibited a polymer concentration of approximately 9.8 wt%, which might lead to intermicellar interactions. The high polymer concentration might shift transitions within the phase diagram or promote the formation of bigger micellar assemblies. Still after dilution, the polymer system seems to have a memory effect as these bigger aggregates are formed despite a considerably lower polymer concentration (0.09 wt%) in comparison to that of the dialyzed sample (0.62 wt%).

In conclusion, we could demonstrate two pathways toward a controlled formation of kinetically frozen nonequilibrium micellar IPEC assemblies. Dilution or dialysis freezes the obtained IPEC structures by a drastic reduction of the concentration of the low molecular weight salt, which in a first step enables inter- and intramicellar exchange processes resulting in the formation of equilibrium morphologies. Thus, IPEC rearrangements are prevented when the solubility conditions for the other polymer compounds are changed, which are in our case altered by the temperature. We could generate spherical and worm-like non-equilibrium IPEC structures, which were colloidally stable at room temperature under the same final conditions (polymer, salt concentration).

In a next step, it would be worthwhile to adapt these approaches to other morphologies and freeze, e.g., vesicles which are formed as equilibrium structure at $T > \text{LCST}$. Therefore, it is necessary to find an appropriate ratio between the block lengths of the charged parts as well as PNIPAM and the water-soluble PEO arm. Such vesicles might then serve as nanocarriers, which release stored molecules upon an increase in salt concentration.

3. References

1. Dähling, C.; Lotze, G.; Drechsler, M.; Mori, H.; Pergushov, D. V.; Plamper, F. A., *Soft Matter* **2016**, *12*, 5127-5137.
2. Dähling, C.; Lotze, G.; Mori, H.; Pergushov, D. V.; Plamper, F. A., *J. Phys. Chem. B* **2017**, *121* (27), 6739-6748.
3. Plamper, F. A.; Murtomäki, L.; Walther, A.; Kontturi, K.; Tenhu, H., *Macromolecules* **2009**, *42* (19), 7254-7257.
4. Mori, H.; Saito, Y.; Takahashi, E.; Nakabayashi, K.; Onuma, A.; Morishima, M., *Polymer* **2012**, *53* (18), 3861-3877.
5. Schneider, C. A.; Rasband, W. S.; Eliceiri, K. W., *Nat. Methods* **2012**, *9* (7), 671-675.
6. Heinz Maier-Leibnitz Zentrum. (2015). KWS-2: Small angle scattering diffractometer. *Journal of large-scale research facilities*, *1*, A29. <http://dx.doi.org/10.17815/jlsrf-1-27>.
7. Doucet, M. SasView Version 4.1. <http://www.sasview.org/>.
8. Guinier, A.; Fournet, G., *Small-Angle Scattering of X-rays*. John Wiley & Sons, Inc.: New York, 1955.
9. Berr, S. S., *J. Phys. Chem.* **1987**, *91* (18), 4760-4765.
10. Ornstein, L. S.; Zernike, F., *Proc. Acad. Sci.* **1914**, *17*, 793-806.
11. Teixeira, J., *J. Appl. Crystallogr.* **1988**, *21*, 781-785.
12. Livsey, I., *J. Chem. Soc., Faraday Trans. 2* **1987**, *83* (8), 1445-1452.
13. Pecora, R., *J. Chem. Phys.* **1968**, *48* (9), 4126-4128.
14. Tirado, M. M.; García de la Torre, J., *J. Chem. Phys.* **1979**, *71* (6), 2581-2587.
15. Tirado, M. M.; García de la Torre, J., *J. Chem. Phys.* **1980**, *73* (4), 1986-1993.
16. Blanazs, A.; Madsen, J.; Battaglia, G.; Ryan, A. J.; Armes, S. P., *J. Am. Chem. Soc.* **2011**, *133* (41), 16581-16587.
17. Plamper, F. A.; Gelissen, A. P.; Timper, J.; Wolf, A.; Zezin, A. B.; Richtering, W.; Tenhu, H.; Simon, U.; Mayer, J.; Borisov, O. V.; Pergushov, D. V., *Macromol. Rapid Commun.* **2013**, *34* (10), 855-860.
18. Kishimura, A.; Koide, A.; Osada, K.; Yamasaki, Y.; Kataoka, K., *Angew. Chem. Int. Edit.* **2007**, *46* (32), 6085-6088.
19. Popescu, M. T.; Korogiannaki, M.; Marikou, K.; Tsitsilianis, C., *Polymer* **2014**, *55* (13), 2943-2951.
20. Bhargava, P.; Tu, Y. F.; Zheng, J. X.; Xiong, H. M.; Quirk, R. P.; Cheng, S. Z. D., *J. Am. Chem. Soc.* **2007**, *129* (5), 1113-1121.
21. Pergushov, D. V.; Müller, A. H. E.; Schacher, F. H., *Chem. Soc. Rev.* **2012**, *41* (21), 6888-6901.
22. Bakeev, K. N.; Izumrudov, V. A.; Kuchanov, S. I.; Zezin, A. B.; Kabanov, V. A., *Macromolecules* **1992**, *25* (17), 4249-4254.